ing from a spontaneous truncation of HIV Env expressed by a recombinant MVA. *Virology* 2008;372:260–72.
39 Vaerman JP, Langendries A, Giffroy D, Brandtzaeg P, Kobayashi K. Lack of SC/pIgR-mediated epithelial transport of a human polymeric IgA devoid of J chain: *in vitro* and *in vivo* studies. *Immunology* 1998;95:90–6.
40 Meckelein B, Externest D, Schmidt MA, Frey A. Contribution of serum immunoglobulin transudate to the antibody immune status of murine intestinal secretions: influence of different sampling procedures. *Clin Diagn Lab Immunol* 2003;10:831–4.
41 Brandtzaeg P. Induction of secretory immunity and memory at mucosal surfaces. *Vaccine* 2007;25:5467–84.
42 Quiding M, Nordström I, Kilander A *et al.* Intestinal immune responses in humans. Oral cholera vaccination induces strong intestinal antibody responses and interferon-gamma production and evokes local immunological memory. *J Clin Invest* 1991;88:143–8.
43 Kozlowski PA, Cu-Uvin S, Neutra MR *et al.* Comparison of the oral, rectal, and vaginal immunization routes for induction of antibodies in rectal and genital tract secretions of women. *Infect Immun* 1997;65:1387–94.
44 Johansson EL, Bergquist C, Edebo A *et al.* Comparison of different routes of vaccination for eliciting antibody responses in the human stomach. *Vaccine* 2004;22:984–90.
45 Johansson EL, Wassén L, Holmgren J *et al.* Nasal and vaginal vaccinations have differential effects on antibody responses in vaginal and cervical secretions in humans. *Infect Immun* 2001;69:7481–6.
46 Mestecky J. The common mucosal immune system and current strategies for induction of immune responses in external secretions. *J Clin Immunol* 1987;7:265–76.
47 Kiyono H, Fukuyama S. NALT- versus Peyer's-patch-mediated mucosal immunity. *Nat Rev Immunol* 2004;4:699–710.
48 Fujihashi K, Staats HF, Kozaki S, Pascual DW. Mucosal vaccine development for botulinum intoxication. *Expert Rev Vaccines* 2007;6:35–45.
49 Streilein JW. Skin-associated lymphoid tissue. *Immunol Ser* 1989;46:73–96.
50 Sontheimer RD. Perivascular dendritic macrophages as immunobiological constituents of the human dermal microvascular unit. *J Invest Dermatol* 1989;93:96S–101S.
51 Bos JD, Kapsenberg ML. The skin immune system: progress in cutaneous biology. *Immunol Today* 1993;14:75–8.
52 Nestle FO, Nickoloff BJ. A fresh morphological and functional look at dermal dendritic cells. *J Cutan Pathol* 1995;22:385–93.
53 Chang SY, Cha HR, Igarashi O *et al.* Cutting edge: Langerin$^+$ dendritic cells in the mesenteric lymph node set the stage for skin and gut immune system cross-talk. *J Immunol* 2008;180:4361–5.

RESEARCH ARTICLE

Human Mutation

OFFICIAL JOURNAL
HGVS
HUMAN GENOME VARIATION SOCIETY
www.hgvs.org

Chemical Chaperone Therapy: Chaperone Effect on Mutant Enzyme and Cellular Pathophysiology in β-Galactosidase Deficiency

Katsumi Higaki,[1]* Linjing Li,[1,2] Udin Bahrudin,[1,3,4] Soichiro Okuzawa,[5] Ayumi Takamuram,[1] Koichi Yamamoto,[1] Kaori Adachi1,[2] Rubigilda C. Paraguison,[1] Tomoko Takai,[1] Hiroki Ikehata,[1] Lika Tominaga,[1] Ichiro Hisatome,[3] Masami Iida,[6] Seiichiro Ogawa,[5] Junichiro Matsuda,[7] Haruaki Ninomiya,[8] Yasubumi Sakakibara,[5] Kousaku Ohno,[2] Yoshiyuki Suzuki,[9] and Eiji Nanba[1]

[1]Division of Functional Genomics, Research Center for Bioscience and Technology, Tottori University, Yonago, Japan; [2]Division of Child Neurology, Department of Neurological Science, Tottori University Faculty of Medicine, Yonago, Japan; [3]Division of Regenerative Medicine and Therapeutics, Institute of Regenerative Medicine and Biofunction, Tottori University Graduate School of Medical Science, Yonago, Japan; [4]Center of Biomedical Research, Medical Faculty Diponegoro University, Semarang, Indonesia; [5]Department of Biosciences and Informatics, Faculty of Science and Technology, Keio University, Kohoku-ku, Yokohama, Japan; [6]Central Research Laboratories, Seikagaku Corporation, Higashi-Yamato, Tokyo, Japan; [7]Laboratory of Animal Models for Human Diseases, National Institute of Biomedical Innovation, Ibaraki, Japan; [8]Department of Biomedical Regulation, School of Health Science, Tottori University, Faculty of Medicine, Yonago, Japan; [9]International University of Health and Welfare Graduate School, Otawara, Japan

Communicated by Hans R. Waterham

Received 10 September 2010; accepted revised manuscript 4 April 2011.
Published online 21 April 2011 in Wiley Online Library (www.wiley.com/humanmutation). DOI 10.1002/humu.21516

ABSTRACT: β-Galactosidase deficiency is a group of lysosomal lipid storage disorders with an autosomal recessive trait. It causes two clinically different diseases, G_{M1}-gangliosidosis and Morquio B disease. It is caused by heterogeneous mutations in the *GLB1* gene coding for the lysosomal acid β-galactosidase. We have previously reported the chaperone effect of *N*-octyl-4-epi-β-valienamine (NOEV) on mutant β-galactosidase proteins. In this study, we performed genotype analyses of patients with β-galactosidase deficiency and identified 46 mutation alleles including 9 novel mutations. We then examined the NOEV effect on mutant β-galactosidase proteins by using six strains of patient-derived skin fibroblast. We also performed mutagenesis to identify β-galactosidase mutants that were responsive to NOEV and found that 22 out of 94 mutants were responsive. Computational structural analysis revealed the mode of interaction between human β-galactosidase and NOEV. Moreover, we confirmed that NOEV reduced G_{M1} accumulation and ameliorated the impairments of lipid trafficking and protein degradation in β-galactosidase deficient cells. These results provided further evidence to NOEV as a promising chaperone compound for β-galactosidase deficiency.
Hum Mutat 32:843–852, 2011. © 2011 Wiley-Liss, Inc.

KEY WORDS: lysosomal storage disease; G_{M1}-gangliosidosis; *GLB1*; chaperone therapy; ubiquitin

Introduction

Acid β-galactosidase (GLB1 or β-gal; EC 3.2.1.23; MIM# 611458) is a lysosomal hydrolase that cleaves the terminal β-gal linkage in ganglioside G_{M1} and other glycoconjugates. Hereditary deficiency of lysosomal β-gal (or β-galactosidosis) is an autosomal recessive lipid storage disorder categorized into two clinical entities, G_{M1}-gangliosidosis (MIM# 230500) and Morquio B disease (MIM# 253010) [Brunetti-Pierri and Scaglia, 2008; Suzuki et al., 2008]. G_{M1}-ganglisidosis is a neurosomatic disease occurring mainly in early infancy or young adults. The infantile form is characterized by rapid progressive psychomotor deterioration, dysmorphism, and macular cherry-red spots. The late-infantile/juvenile form shows a milder clinical course without remarkable bone changes or visceromegaly. The adult or chronic form is uncommon with a more protracted clinical course. Morquio B disease is a rare bone disease without central nervous system involvement.

The human *GLB1* gene (MIM# 611458) encoding β-gal protein is composed of 16 exons and is mapped on 3p21.33 [Morreau et al., 1989; Oshima et al., 1988]. It expresses two alternatively spliced mRNAs, a major product for lysosomal β-gal and a minor product for elastin-binding protein. To date, more than 130 mutations have been reported in *GLB1* and common mutations have been found in some types of β-gal deficiency: I51T and R201H for adult G_{M1}-gangliosidosis, R201C for juvenile G_{M1}-gangliosidosis, and W273L for Morquio B disease [Brunetti-Pierri and Scaglia, 2008; Hofer et al., 2009, 2010; Suzuki et al., 2008].

The pathophysiological hallmark of this disease is a lysosomal accumulation of G_{M1}-ganglioside and its derivatives in neurons of the brain and a high amount of oligosaccharides in visceral organs

Additional Supporting Information may be found in the online version of this article.

*Correspondence to: Katsumi Higaki, Division of Functional Genomics, Research Center for Bioscience and Technology, Tottori University, 86 Nishi-cho, Yonago, 683-8503, Japan. E-mail: kh4060@med.tottori-u.ac.jp

Contract grant sponsor: Ministry of Education, Culture, Science, Sports and Technology of Japan; Contract grant numbers: 18390299; 20790728; 21659257; Contract grant sponsor: Ministry of Health, Labour and Welfare of Japan; Contract grant numbers: H10-No-006; H14-Kokoro-017; H17-Kokoro-019; H20-Kokoro-022, and a grant for Research for Intractable Diseases; Contract grant sponsor: The Japan Health Sciences Foundation.

and urine [Brunetti-Pierri and Scaglia, 2008; Suzuki et al., 2008]. Impaired autophagy and proteasome function has been shown to be related to pathogenesis of several lysosomal storage diseases (LSDs) including G_{M1}-gangliosidosis [Otomo et al., 2009; Settembre et al., 2008; Takamura et al., 2008]. Autophagic dysfunction leads to enhanced susceptibility to mitochondria-mediated apoptosis and to oxidative stress that activates inflammation processes [Luciani et al., 2010; Takamura et al., 2008].

At present, no specific therapy is available for patients with β-gal deficiency. Enzyme replacement therapy has been introduced for the treatment of Gaucher disease and other LSDs but is not applicable for the brain pathology of β-gal deficiency [Brady and Schiffmann, 2004]. Gene therapy has been shown to be of limited effect on bone and brain manifestations of β-gal deficiency [Takaura et al., 2005]. We have developed chemical chaperone (or pharmacological chaperone) therapy for LSDs [Fan et al., 1999; Iwasaki et al., 2006; Matsuda et al., 2003; Suzuki et al., 2007]. In this therapy, competitive enzyme inhibitors with a low molecular weight bind and stabilize the mutant protein in the endoplasmic reticulum (ER) and facilitate its transport to the lysosome [Parenti, 2010; Suzuki et al., 2009]. We have identified a novel valienaimine derivative, *N*-octyl-4-epi-β-valienamine (NOEV) as a potent chemical chaperone for mutant β-gal proteins [Matsuda et al., 2003; Ogawa et al., 2002]. Our initial study has shown that NOEV increased mutant β-gal activity in cultured fibroblasts and in the brain of G_{M1}-gangliosidosis mouse model [Iwasaki et al., 2006; Suzuki et al., 2007].

In this study, we have examined the chaperone effect of NOEV on human mutant β-gal proteins and cellular pathophysiology of affected cells.

Materials and Methods

Materials

Dulbecco's Modified Eagle's Medium (DMEM) and DMEM/F12 were obtained from Wako (Tokyo, Japan). Fetal bovine serum (FBS) was from HyClone Lab (Waltham, MA). Lipofectamine 2000 transfection reagent was from Invitrogen Corp. (Carlsbad, CA). NOEV was synthesized in Central Research Lab, Seikagaku Corp (Tokyo, Japan). Mouse monoclonal anti-ubiquitin (Ub; P4D1) and rabbit polyclonal anti-β-tubulin were purchased from Santa Cruz Biotech. Inc. (Santa Cruz, CA). Mouse monoclonal anti-G_{M1} (GMB16) was from Seikagaku Corp. (Tokyo, Japan). Rabbit polyclonal anti-p62/SQSTM1 (PM045) was from MBL Co. Ltd (Nagoya, Japan). Mouse monoclonal anti-golgin 97 (CDF4) and BODIPY FL C5-ceramide were from Molecular Probes (Invitrogen Corp., Carlsbad, CA). OptiPrep density gradient medium was from Axis-Shield (Oslo, Norway). 4-Methylumbelliferone (4-MU)-conjugated β-D-galactoside, α-D-galactoside, N-acetyl-β-D-glucosaminide and G_{M1} from bovine brain were from Sigma (St. Louis, MO).

Mutational Analysis

Total genome DNA was extracted from blood or harvested cultured primary skin fibroblasts from G_{M1}-gangliosidosis patients using a standard phenol-chloroform extraction procedure. DNA samples from healthy subjects were used as normal controls for heteroduplex formation. Polymerase chain reaction (PCR) amplification spanning from exons 1 to 16 of *GLB1* gene was performed using a number of primer sets (Supp. Table S1). All exons and flanking sequences of *GLB1* were screened for mutations by denaturing high-performance liquid chromatography (DHPLC, Transgenomic WAVE System, Omaha, NE) as described in Supp. Methods. Mutations were confirmed by direct sequencing (ABI 3130xl, Applied Biosystems, Foster City, CA) and were presented with a unified numbering system based on the sequence of GenBank entry NM_000404.2. The gene analysis of the patients was carried out according to the "Guidelines for Genetic Testing" by Genetic Medicine-Related Society in Japan.

Construction of Human β-Gal Expression Plasmids

Human β-gal cDNA (2.1 kb) was subcloned into a mammalian expression vector pCMV-Script (Stratagene, La Jolla, CA) [Oshima et al., 1988]. Mutations were introduced by Quick Change II site-directed mutagenesis (Stratagene) using oligonucleotide primers (Supp. Tables S2 and S3) following the manufacturer's protocol. All the 94 mutations (87 missense and 7 nonsense or frame shift mutations) were confirmed by sequencing. For transfection experiments, plasmid DNA was obtained using Plasmid DNA purification kit (Qiagen, Hilden, Germany).

Cell Culture, Transfection, and NOEV Treatment

Human skin fibroblasts from patients with β-gal deficiency were obtained in our laboratories or provided by colleagues at medical and scientific institutes (Supp. Methods). Human fibroblasts and mouse fibroblast cell lines from β-gal knockout (KO) mouse embryo [Matsuda et al., 2003] were cultured in DMEM supplemented with 10% FBS. Transfection was performed using Lipofectamine 2000 reagent following the manufacturer's protocol with minor modification. Briefly, β-gal-deficient mouse fibroblasts were prepared in 35-mm cultured dishes and transfected with a mixture of 2 μg of β-gal expression plasmids and 5 μl of Lipofectamine 2000 reagent. After 5 hr of incubation, cultured medium was replaced fresh medium with or without NOEV and cells were incubated for 48 hr. Mock pCMV-script DNA was used as a negative control. For human skin fibroblasts, cells from normal and six strains were cultured with or without NOEV and were incubated for 96 hr as described before [Iwasaki et al., 2006].

Lysosomal Enzyme Assay

Lysosomal enzyme activity in cell lysate was measured by using 4-MU substrates as described previously [Iwasaki et al., 2006]. Briefly, cells in 35-mm dishes were washed with phosphate-buffered saline (PBS) (4°C) and scraped into 100 μl 0.1% Triton X-100 in dH_2O. After centrifugation (6,000 rpm for 15 min at 4°C) to remove insoluble materials, 10 μl of lysates with 20 μl of the substrate solution in 0.1 M citrate buffer (pH 4.5) was incubated at 37°C for 30 min and the reaction was terminated by adding 0.2 M glycin-NaOH buffer (pH 10.7). The librated 4-MU was measured with a fluorescence plate reader (excitation 340 nm; emission 460 nm; Infinite F500, TECAN Japan, Kawasaki, Japan). Protein concentrations were determined using Protein Assay Rapid Kit (Wako, Tokyo, Japan) and enzyme activity was normalized by protein concentration.

Inhibition and Stabilization of β-Gal In Vitro

Cell lysates in 0.1% Triton X-100 in dH_2O from normal and patient (R201C/R201C) skin fibroblasts were used for in vitro analysis. For inhibition assay, lysates were mixed with 4-MU β-gal substrates in the absence or presence of increasing concentrations of NOEV. For heat stabilization, they were incubated in 0.1 M citrate buffer (pH 7) at 48°C for the time indicated, and then incubation was terminated by adding 2 volumes of 0.1 M citrate buffer (pH 4.5). The β-gal activity was measured as described above.

Protein Extraction, Subcellular Fractionation, and Western Blotting

Cells were lysed by sonication in 10 mM Tris-HCl (pH 7.4), 150 mM NaCl, 1 mM EDTA, 1 mM EGTA, 1% Triton X-100, and a protease inhibitor cocktail (Roche Diagnostics, Indianapolis, IN) and the supernatants were used as total extracts. For subcellular fractionation, extracted proteins were subjected to continuous gradient ultracentrifugation (90,000 × *g* for 20 hr at 4°C in SW 41Ti rotor) in OptiPrep gradient (Axis-Shield, Norway) as described previously [Sugii et al., 2003]. The top 20 fractions of the gradients were recovered and subjected to β-gal enzyme assay and Western blotting. Western blotting was performed as described previously [Otomo et al., 2009; Takamura et al., 2008]. Signals from horseradish peroxidase-conjugated secondary antibodies were visualized by ECL detection kit (GE Healthcare Bioscience, Piscataway, NJ) and images were obtained using LAS-4000 lumino image analyzer (Fujifilm, Tokyo, Japan).

Fluorescence Staining

All the procedures were carried out at room temperature as described previously [Otomo et al., 2009; Takamura et al., 2008]. Cultured cells were fixed with 4% paraformaldehyde in PBS for 30 min. They were permeabilized with 0.1% Triton X-100 in PBS for 15 min, blocked with 1% bovine serum albumin (BSA) for 1 hr, and incubated with primary antibodies for 1 hr. We used anti-G_{M1} at 1:50 dilution with 0.1% BSA/PBS. Bound antibodies were detected with Alexa-Fluor-conjugated secondary antibodies (diluted with 1:2,000 in 0.1% BSA/PBS) for 1 hr. Slides were coverslipped with Vectashild mounting media (Vector Laboratories, Burlingame, CA) and fluorescence images were obtained sequentially using a confocal laser microscopy (Leica TCS SP-2; Wetzler, Germany).

BODIPY-Cer Labeling

Prior to labeling, cells on the coverslip were incubated with 0.2 μM G_{M1} for 48 hr. They were then incubated with 5 μM BODIPY FL C5-Cer-BSA in Hank's-balanced salt solution for 30 min at 37°C, washed, and incubated in fresh medium for 30 min at 37°C. Then cells were fixed and stained with anti-golgin97. Fluorescence images were obtained using a confocal microscopy.

Molecular Simulation of Human β-Gal Structure and Its Interaction with NOEV

The three-dimensional structure of human β-gal enzyme protein was predicted using a sequence alignment of human and *Penicillium* sp. β-gal, and a homology modeling method 3D-JUDY [Suzuki et al., 2009]. The conformation of human β-gal and NOEV complex was computed by AUTODOCK4. The conformation was subjected to further structural optimization.

Primary Culture of Astrocytes from Mouse Brains

C57BL/6-based congenic strain KO mouse with β-gal deficiency and KO-Tg (knockout-transgenic) mice (I51T and R201C mice) that express human mutant I51T or R201C enzyme protein have been established and characterized by us [Matsuda et al., 1997, 2003]. All procedures were carried out according to the protocols approved by the committee for animal experiments in Tottori University. Primary astrocytes were cultured as described previously [Takamura et al., 2008]. Briefly, brains were removed from postnatal day 4 mice under anesthesia. The cerebral cortex was dissociated and cells were seeded on plastic dishes in DMEM/F12 supplemented with 15% FBS. They were cultured for 7 days, trypsinized, and seeded on dishes with DMEM-F12 with 10% FBS. They were confirmed to be GFAP-positive astrocytes at 3 weeks (data not shown).

Results

Mutation Analysis of G_{M1}-Gangliosidosis Patients

The DHPLC and sequence analyses identified 46 mutation alleles including 9 novel mutations in 26 patients with G_{M1}-gangliosidosis (Supp. Fig. S1 and Table 1).

Characterization of NOEV Effects in Cell Lysate from Human Skin Fibroblasts

Chemical structure of NOEV is shown in Figrue 1A [Ogawa et al., 2002]. NOEV inhibited β-gal activity in cell lysates of cultured human skin fibroblasts at pH 5 (Fig. 1B). It was effective both in cells from normal and R201C/R201C patient with IC_{50} values of 0.125 and 0.132 μM, respectively, at pH 5 (Fig. 1B). NOEV has no effects on α-gal or β-hexosaminidase (β-hex) under the same conditions. To evaluate in vitro NOEV effects on enzyme stabilization, lysates were preincubated with increasing concentrations of NOEV and were subjected to heat inactivation (48°C) at pH 7.0. In the absence of NOEV, the activities of normal and R201C β-gal decreased to 11 and 7% after a 30-min incubation, respectively. NOEV ameliorated these decreases in a dose-dependent manner (Fig. 1C).

Chaperone Effects of NOEV in Cultured Human Skin Fibroblasts

To evaluate the chemical chaperone effect of NOEV in cultured human skin fibroblasts, cells were cultured in the medium with increasing concentrations of NOEV for 96 hr, and the β-gal enzyme activity in cell lysates was determined. In the six lines with β-gal deficiency, we found significant chaperone effects of NOEV in three lines, which contained β-gal mutations of G190D/G190D (patient #18), R201C/R201C and R457Q/R457Q. NOEV had no effects in cells with β-gal mutations of I51T/I51T, I51T/Y316C (patient #24) and G438E/G438E (Fig. 2A). To examine whether NOEV enhanced trafficking of the mutant enzyme protein to the lysosomes, we performed the subcellular fractionation experiments. Immunoblot analyses of each fraction showed the localization of the ER marker calnexin in fractions #1–4 and that of the lysosome marker lamp-2 in fractions #12–16, and the localization of these markers were indistinguishable between control and R201C/R201C cells (data not shown). In fractions from control cells, the β-gal activity was recovered mainly in fractions #12–17 (data not shown). The same analysis of R201C/R201C cell fractions showed broad distribution of β-gal activity with peaks at #1 and #15 (Fig. 2B). NOEV treatment of R201C/R201C cells increased the activity up to four folds in #12–16, which suggested increased transport of mutant protein to the late endosomes/lysosomes in cells treated with NOEV.

Intracellular Trafficking of BODIPY-Ceramide

We also examined trafficking of fluorescence-labeled ceramide. BODIPY-labeled ceramide was internalized and subsequently

Table 1. Mutations in *GLB1* Gene Causing G_{M1}-Gangliosidosis

Patient	Nucleotide change[a]	Predicted aa change	Clinical phenotype	Ethnic origin	References
1	c.1438A>G	p.M480V	Inf G_{M1}	Japanese	This study
	c.1445G>A	p.R482H			Mosna et al. [1992]
2	c.442C>T	p.R148C	Inf G_{M1}	Japanese	Nishimoto et al. [1991]
	?	?			(−)
3	c.622C>T	p.R208C	Inf G_{M1}	Japanese	Boustany et al. [1993]
	c.622C>T	p.R208C			Boustany et al. [1993]
4	c.176G>A	p.R59H	Inf G_{M1}	Japanese	Silva et al. [1999]
	c.996C>G	p.D332E			Hofer et al. [2009]
5	c.1445G>A	p.R482H	Inf G_{M1}	Japanese	Mosna et al. [1992]
	c.1646C>T	p.P549L			Santamaria et al. [2007]
6	c.276−277insG	p.P93AfsX7	Inf G_{M1}	Japanese	This study
	?	?			(−)
7	c.542T>A	p.I181K	Inf G_{M1}	Turkish	Hofer et al. [2010]
	c.542T>A	p.I181K			Hofer et al. [2010]
8	c.601C>T	p.R201C	Adul G_{M1}	unknown	Oshima et al. [1991]
	c.602G>A	p.R201H			Oshima et al. [1995]
9	c.161G>T	p.S54I	Inf G_{M1}	unknown	This study
	?	?			(−)
10	c.175C>T	p.R59C	Adul G_{M1}	unknown	Caciotti et al. [2005]
	c.245C>T	p.T82M			Chakraborty et al. [1994]
11	c.601C>T	p.R201C	Adul G_{M1}	Japanese	Oshima et al. [1991]
	c.1259C>A	p.T420K			Santamaria et al. [2006]
12	c.145C>T	p.R49C	Inf G_{M1}	Estonian	Nishimoto et al. [1991]
	c.391G>A	p.E131K			This study
13	c.601C>T	p.R201C	Inf G_{M1}	Estonian	Oshima et al. [1991]
	c.808T>G	p.Y270D			Paschke et al. [2001]
14	c.1343A>T	p.D448V	Inf G_{M1}	Japanese	Hofer et al. [2010]
	c.1746G>A	p.W582X			This study
15	c.176G>A	p.R59H	Inf G_{M1}	Japanese	Silva et al. [1999]
	c.1820T>C	p.L608P			This study
16	c.436_438delCTT	p.L146del	Inf G_{M1}	Japanese	This study
	?	?			(−)
17	c.176G>A	p.R59H	Inf G_{M1}	UAE	Silva et al. [1999]
	c.176G>A	p.R59H			Silva et al. [1999]
18	c.569G>A	p.G190D	Inf G_{M1}	Turkish	Hofer et al. [2009]
	c.569G>A	p.G190D			Hofer et al. [2009]
19	c.276G>A	p.W92X	Inf G_{M1}	Indian	This study
	c.276G>A	p.W92X			This study
20	c.75+2_3insT		Inf G_{M1}	Belgian	Chakraborty et al. [1994]
	c.75+2_3insT				Chakraborty et al. [1994]
21	c.569G>A	p.G190D	Inf G_{M1}	Turkish	Hofer et al. [2009]
	c.569G>A	p.G190D			Hofer et al. [2009]
22	c.569G>A	p.G190D	Inf G_{M1}	Turkish	Hofer et al. [2009]
	c.569G>A	p.G190D			Hofer et al. [2009]
23	c.841C>T	p.H281Y	Inf G_{M1}	Russia	Paschke et al. [2001]
	?	?			(−)
24	c.152T>C	p.I51T	Adul G_{M1}	Japanese	Oshima et al. [1991]
	c.947A>G	p.Y316C			Oshima et al. [1991]
25	c.428_429insA	p.S144VfsX42	Inf G_{M1}	British	This study
	?	?			(−)
26	c.602G>A	p.R201H	Adul G_{M1}	Belgian	Oshima et al. [1995]
	c.1441G>T	p.G481X			Santamaria et al. [2006]

[a]The numbering for the nucleotide changes are based on cDNA sequence with GenBank entry NM_000404.2. with +1 corresponding to the A of ATG translation initiation codon in the reference sequence.

transported to the Golgi complex in normal cells. In consistence with the previous reports [Marks and Pagano, 2002; Puri et al., 1999], it was localized to the perinuclear punctuates in affected cells when cells were cultured with G_{M1} (Fig. 2C). NOEV treatment restored the transport of BODIPY-ceramide to the Golgi apparatus in G190D/G190D (patient #18), R201C/R201C and R457Q/R457Q cells, but not in I51T/I51T and G438E/G438E cells.

Screening of NOEV Effects on Human Mutant β-Gal Proteins

We next screened NOEV effects on 94 different β-gal mutants (Supp. Table S2) by using transient expression in β-gal-deficient fibroblasts. After trasfection, cells were incubated with increasing concentrations of NOEV for 48 hr and the β-gal in cell lysates was determined. 22 missense mutants responded to NOEV (Fig. 3 and Supp. Fig. S2). The maximum response was obtained at 2 μM in most of the responsive mutants except for 7 (L173P, N318H, D332E, Y444C, R457Q, R590C, and R590H). Several mutants (D214Y, W273R, N318H, Y347C, Y444C, and R590H) showed high residual activities (more than 10% of normal activity). The tertiary structure of human β-gal protein was predicted by homology modeling using *Penicillium* sp. β-gal as a template and the interaction between β-gal protein and NOEV was predicted by AUTODOCK4 [Jo et al., 2010; Suzuki et al., 2009]. The mutations responsive to NOEV were localized throughout the various

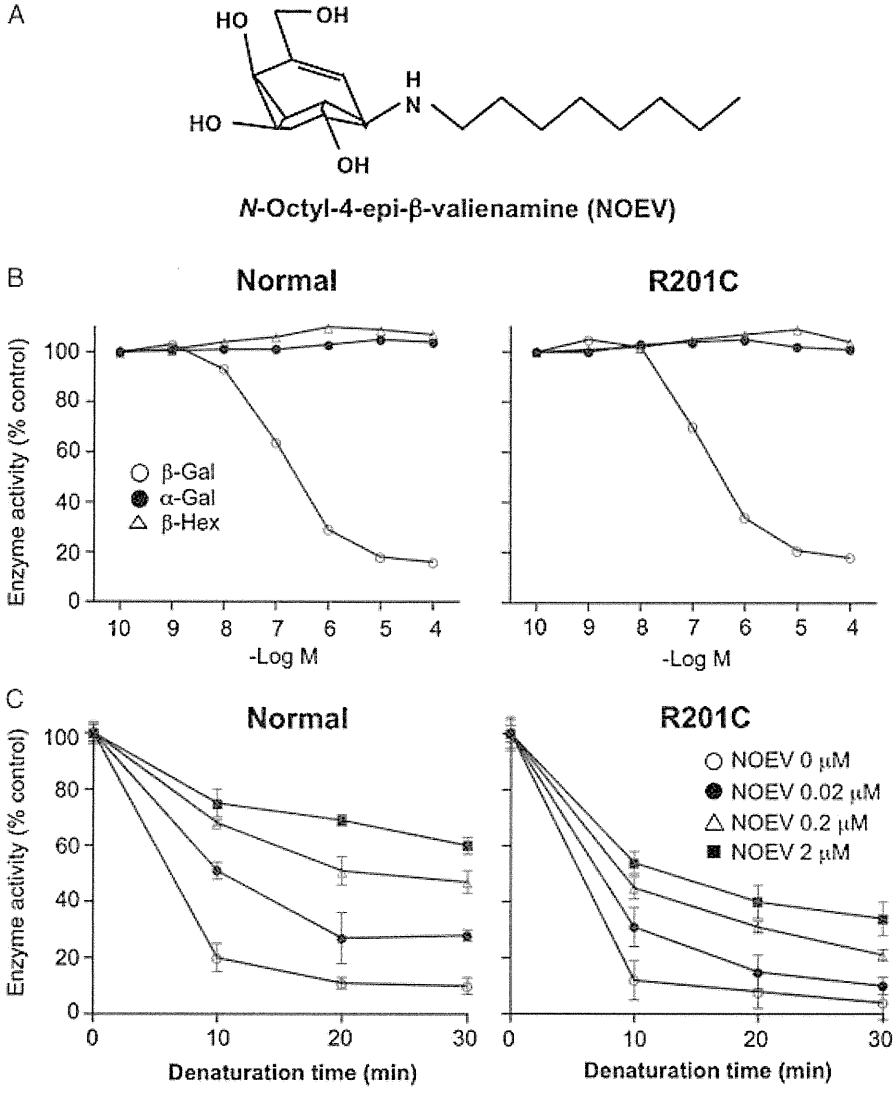

Figure 1. NOEV binds to and stabilizes human β-galactosidase proteins in vitro. **A:** Structure of NOEV. **B:** Enzyme activities in cell lysates from normal and patient fibroblast with R201C/R201C mutations were determined after incubation with or without NOEV. **C:** Cell lysates were incubated at pH 7.0 and 48°C for the indicated time and the β-gal activity was measured. Each point represents means of triplicates obtained in at least three independent experiments. Values were expressed as relative to the activity in the absence of NOEV as 100%.

protein regions including triosephosphateisomerase (TIM) motif (Fig. 4) [Kang and Stevens, 2009].

NOEV Reduced G_{M1} Accumulation and Protein Ubiquitination in Primary Cultured Mouse Astrocytes Expressing R201C β-Gal

G_{M1} is enriched in the plasma membrane lipid microdomain (also known as lipid rafts), particularly in neurons and astrocytes. Because fibroblasts do not accumulate G_{M1} to the same extent as neuronal cells, we next investigated NOEV effects using astrocytes isolated from mouse brain. The activity of β-gal was undetectable in β-gal$^{-/-}$ astrocytes, but some activities were detected in R201C and I51T cells (Fig. 5A). Immunostaining with anti-G_{M1} showed lysosomal G_{M1} accumulation in these cells, whereas no such staining was detected in wild-type (wt) astrocytes (Fig. 5B). Treatment with 0.2 μM NOEV increased the enzyme activity and reduced G_{M1} accumulation in R201C cells, indicating the effectiveness of NOEV as shown in fibroblasts. Although NOEV significantly reduced β-gal activity in the wt cells, no such effect was observed in β-gal$^{-/-}$ and I51T cells.

We and others have proposed that impairments of the protein degradation pathways play an important role in neurodegeneration of several lysosomal storage diseases [Otomo et al., 2009; Settembre et al., 2008; Takamura et al., 2008]. p62, also known as sequestosome-1 is an adaptor protein, initially isolated as an interacting partner of atypical proteins kinase C [Sanchez et al., 1998]. Recent studies suggest that p62 is a ubiquitin- and LC3-binding protein, that regulates the formation of protein aggregates and is removed by autophagy [Ichimura et al., 2008; Komatsu et al., 2007]. Immunofluorescence analysis in astrocytes revealed that p62 accumulated in β-gal$^{-/-}$ and R201C but not in wt cells, and NOEV significantly reduced p62 accumulation in R201C cells (Fig. 5C). No change was observed in p62 protein levels in wt and β-gal$^{-/-}$ cells after NOEV treatment. These results were confirmed in immunoblot analysis of cell lysates from astrocytes (Fig. 5D).

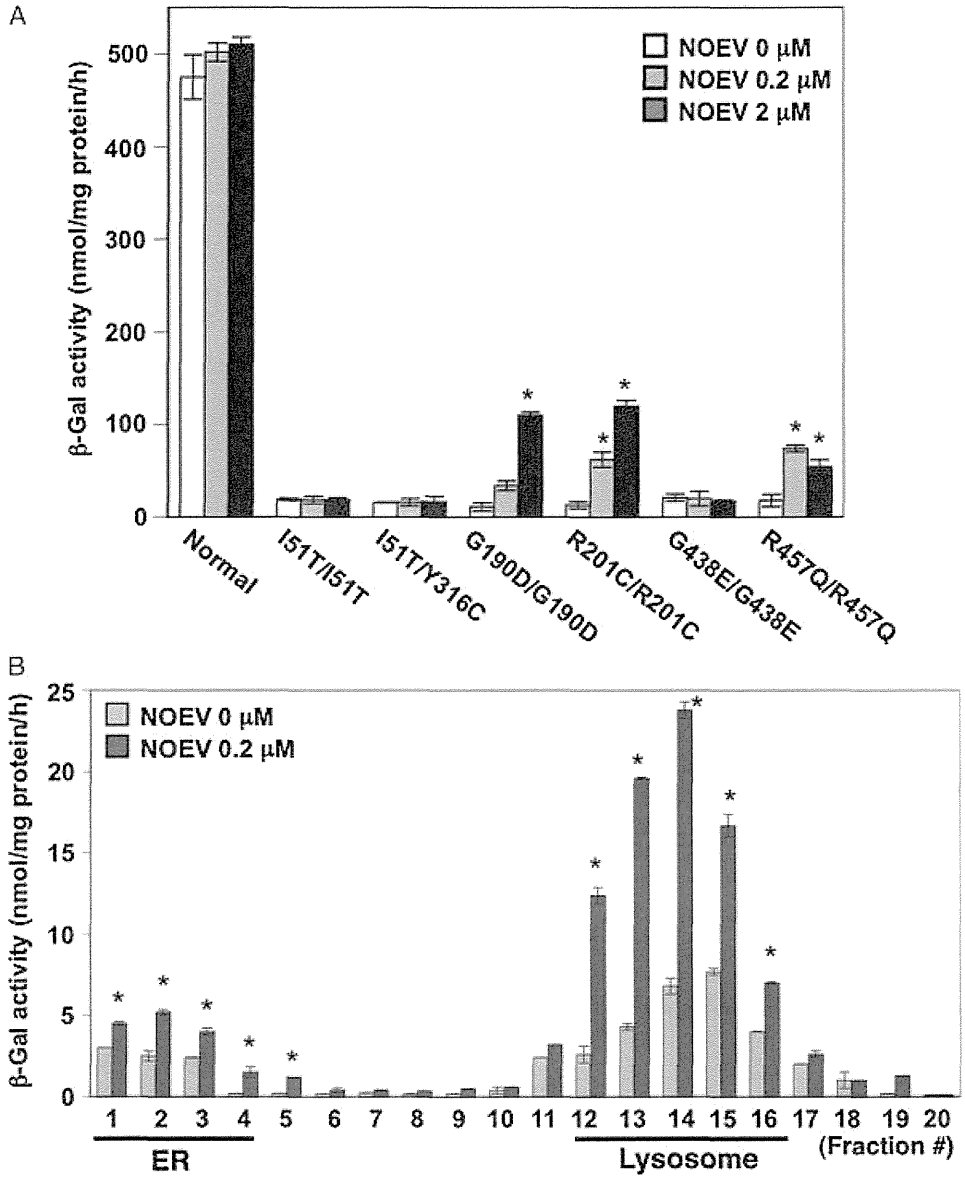

Figure 2. Effects of NOEV on human skin fibroblasts from patients with β-galactosidase deficiency. **A:** Cells were incubated in the absence or presence of NOEV for 96 hr and the β-gal activity in lysates were measured (I51T/Y316C; patient #24 and G190D/G190D; patient #18). **B:** Fibroblasts from patient with R201C/R201C were cultured with or without NOEV for 96 hr and cell lysates were subjected to Opti-prep fractionation as described in Materials and Methods. Each fraction was assessed for β-gal activity. Each bar represents the mean ± SEM of three determinations each done in triplicate. $^*P<0.05$, statistically different from the values in the absence of NOEV. **C:** Cells were cultured with or without NOEV for 96 hr and subjected to BODIPY-Cer and anti-golgin97 labeling. Representative images were obtained under confocal microscope. Bar = 20 μm.

Moreover, upregulation of ubiquitinated proteins in lysate from R201C astrocyte was significantly ameliorated after NOEV treatment (Fig. 5E).

Discussion

To date, more than 130 mutations in *GLB1* have been identified as disease causing [Brunetti-Pierri and Scaglia, 2008; Hofer et al., 2009, 2010; Suzuki et al., 2008], of which approximately 75% cause amino acid substitutions. Some of the mutant proteins have normal or near-normal activity, but they are unstable at neutral pH in the ER/Golgi apparatus because of inappropriate molecular folding, and are rapidly degraded by intracellular quality control systems [Fan et al., 1999; Suzuki et al., 2009]. Because most of the novel mutations (except for S54I, E131K, and L608P) identified in this study caused premature termination or frame shift, they showed no response to NOEV.

In our initial study, we identified NOEV as a potent inhibitor of human β-gal, and confirmed its chaperone effect [Iwasaki et al., 2006; Matsuda et al., 2003; Suzuki et al., 2007]. In this study, we characterized the effect of NOEV on lysosomal trafficking of mutant R201C protein and on lipid trafficking in patients' fibroblasts. A novel compound, DLHex-DGJ, which is an *N*-alkaylated derivative of 1-deoxygalactonojirimycin, was recently reported to act as a chaperone for mutant β-gal at much higher concentrations than NOEV [Fantur et al., 2010].

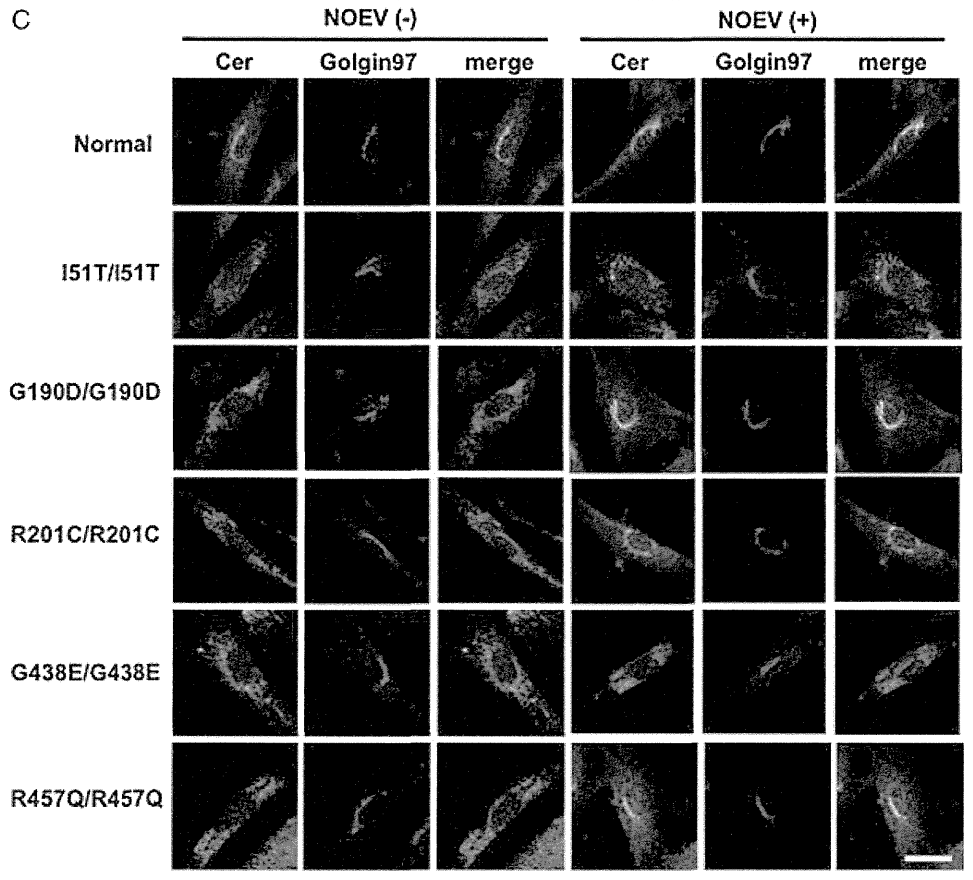

Figure 2. Continued.

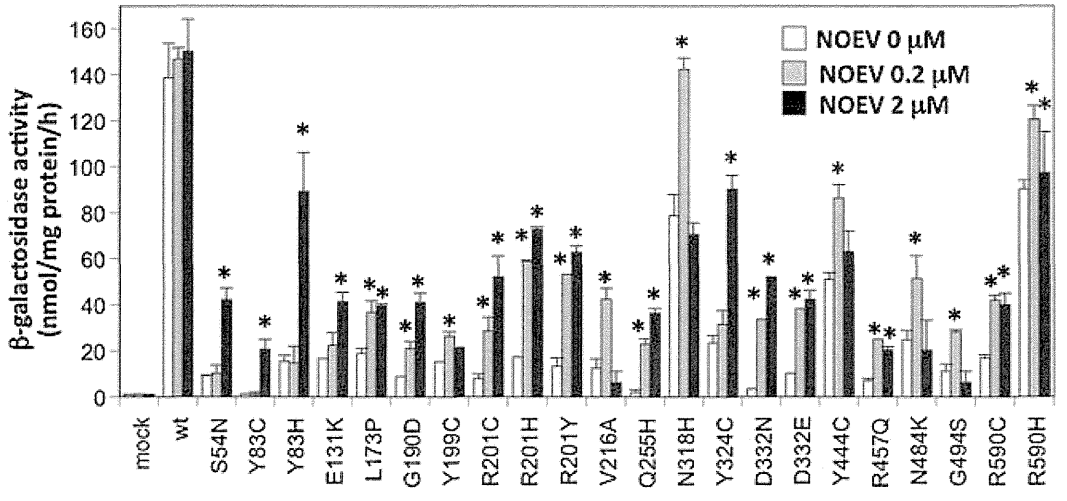

Figure 3. Screening of NOEV effects on human mutant β-galactosidase. β-Gal-deficient mouse fibroblasts were transiently transfected with human normal or mutant β-gal cDNA and incubated with or without NOEV for 48 hr. Cell lysates were assessed for β-gal activity. Mock tranfection was used as a control. Each bar represents the mean ± SEM of three determinations each done in triplicate. $^*P<0.05$, statistically different from the values in the absence of NOEV.

To evaluate NOEV effects on different mutations, we performed transient transfection experiments and found that 23% of the mutants examined were responsive to NOEV. Many of these mutations were found in juvenile and infantile form of G_{M1}-gangliosidosis. We estimate that NOEV therapy would be effective in approximately 30–40% of the patients. Although several mutants (D214Y, W273R, N318H, Y347C, and R590H) showed relatively high residual activities, this is most likely

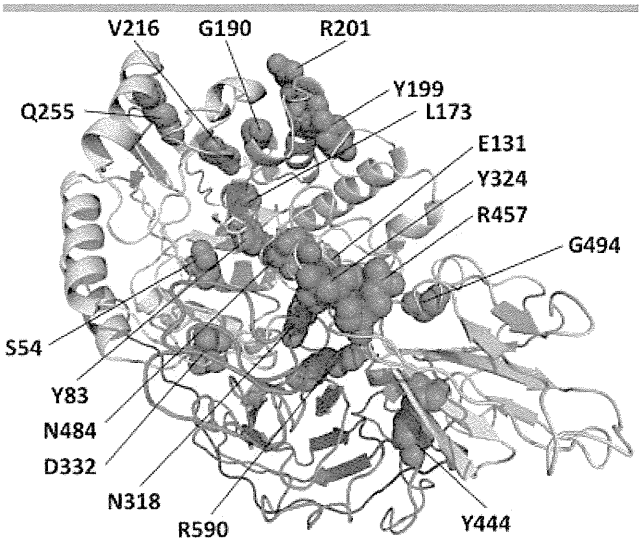

Figure 4. Structural model of human β-galactosidase protein and its interaction with NOEV. The tertiary structure of human β-gal protein and its interaction with NOEV were predicted by computational analyses as described in Materials and Methods. NOEV is colored in yellow. Red circles represent location of residues responsive to NOEV. A blue region represents a typical TIM barrel including the active site.

because of the overexpression of the mutant proteins. Both human skin fibroblasts and transfected cells will be necessary for future screening of chaperone effects [Iwasaki et al., 2006].

The structure of lysosomal enzyme proteins has been determined either by crystal diffraction analysis or homology modeling [Dvir et al., 2003; Garman and Garboczi, 2004; Kang and Stevens, 2009; Lemieux et al., 2006; Rempel et al., 2005]. Molecular interaction of some lysosomal enzymes with their respective chaperones has been resolved [Flanagan et al., 2009; Jo et al., 2010; Lieberman et al., 2009]. These studies revealed that chaperone compounds bind and restore protein conformation of N370S mutant β-glu protein [Lieberman et al., 2009; Lin et al., 2004; Sawkar et al., 2002]. In the current study, we used a predicted structural model and thus we have not obtained the statistical significance. A crystal structure of the β-gal protein would be warranted for further study.

Various pathophysiological changes including impaired calcium homeostasis, elevated levels of inducible nitric oxide synthase, activation of inflammation cascades, accumulation of undegraded proteins, and elevation of ER stress have been shown in the brain of G_{M1}-gangliosidosis model mouse [Jeyakumar et al., 2003; Sano et al., 2009; Tessitore et al., 2004], and alteration in lipid trafficking has been shown in fibroblasts from G_{M1}-gangliosidosis patients [Marks and Pagano, 2002; Puri et al., 1999]. Then we examined the relevance of NOEV on the pathophysiology at the cellular level, and found that NOEV clearly reduced G_{M1} accumulation in R201C astrocytes. Besides, accumulations of p62 and ubiquitinated proteins in R201C astrocytes were effectively suppressed by NOEV providing further evidence on the efficacy of NOEV.

In summary, we found 22 missense mutations responsive to NOEV chaperone effects. We also confirmed that NOEV restored several of cellular functions in the affected cells. These results provide further evidence that NOEV is a promising chaperone compound for β-gal deficiency.

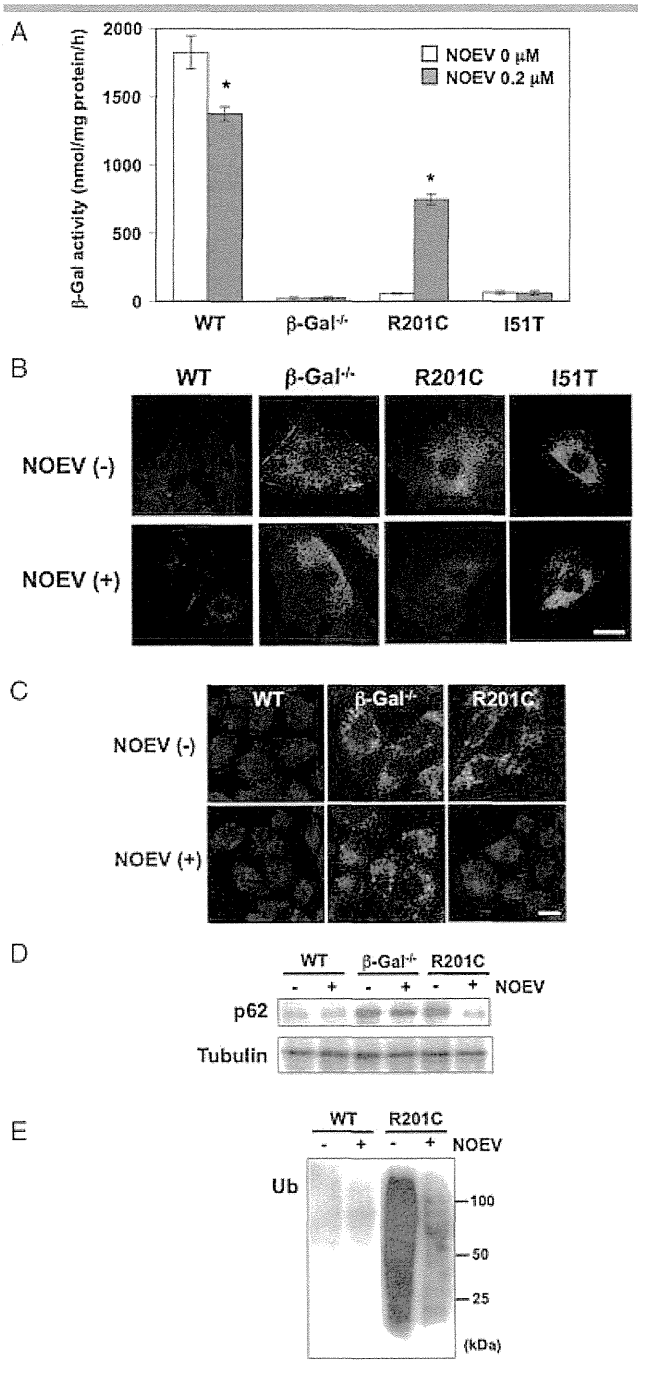

Figure 5. NOEV reduces G_{M1} and ubiquitin accumulation in primary astrocyte from R201C mouse brain. **A:** Chaperone effect of NOEV on R201C primary astrocytes. Each point represents means of triplicates obtained in at least three independent experiments. $^*P<0.05$, statistically different from the value in the absence of NOEV. **B:** Immunostaining with anti-G_{M1}. Cytoplasmic lysosomal accumulation of G_{M1} was observed in R201C astrocytes and it was diminished by NOEV. **C:** Immunostining with anti-p62. Bar = 20 μm. **D** and **E:** Immunoblotting with anti-p62 and tubulin (D), and with anti-ubiquitin (E).

References

Boustany RM, Qian WH, Suzuki K. 1993. Mutations in acid beta-galactosidase cause GM1-gangliosidosis in American patients. Am J Hum Genet 53:881–888.

Brady RO, Schiffmann R. 2004. Enzyme-replacement therapy for metabolic storage disorder. Lancet Neurol 3:752–756.

Brunetti-Pierri N, Scaglia F. 2008. G_{M1}-gangliosidosis: review of clinical, molecular, and therapeutic aspects. Mol Genet Metab 94:391–396.

Caciotti A, Donati MA, Bardelli T, d'Azzo A, Massai G, Luciani L, Zammarchi E, Morrone A. 2005. Primary and secondary elastin-binding protein defect leads to impaired elastogenesis in fibroblasts from GM1-gangliosidosis patients. Am J Pathol 167:1689–1698.

Chakraborty S, Rafi MA, Wenger DA. 1994. Mutations in the lysosomal beta-galactosidase gene that cause the adult form of GM1 gangliosidosis. Am J Hum Genet 54:1004–1013.

Dvir H, Harel M, McCarthy AA, Toker L, Silman I, Futerman AH, Sussman JL. 2003. X-ray structure of human acid-beta-glucosidase, the defective enzyme in Gaucher disease. EMBO Rep 4:704–709.

Fan JQ, Ishii S, Asano A, Suzuki Y. 1999. Accelerated transport and maturation of lysosomal alpha-galactosidase A in Fabry lymphoblasts by en enzyme inhibitor. Nat Med 5:112–115.

Fantur K, Hofer D, Schitter G, Steiner AJ, Pabst BM, Wrodnigg TM, Stütz AE, Paschke E. 2010. DLHex-DGJ, a novel derivative of 1-deoxygalactonojirimycin with pharmacological chaperone activity in human G(M1)-gangliosidosis fibroblasts. Mol Genet Metab 100:262–268.

Flanagan JJ, Rossi B, Tang K, Wu X, Mascioli K, Donaudy F, Tuzzi MR, Fontana F, Cubellis MV, Porto C, Benjamin E, Lockhart DJ, Valenzano KJ, Andria G, Parenti G, Do HV. 2009. The pharmacological chaperone 1-deoxynojirimycin increases the activity and lysosomal trafficking of multiple mutant forms of acid alpha-glucosidase. Hum Mutat 30:1683–1692.

Garman SC, Garboczi DN. 2004. The molecular defect leading to Fabry disease: structure of human alpha-galactosidase. J Mol Biol 337:319–335.

Hofer D, Paul K, Fantur K, Beck M, Bürger F, Caillaud C, Fumic K, Ledvinova J, Lugowska A, Michelakakis H, Radeva B, Ramaswami U, Blecko B, Paschke E. 2009. G_{M1}-gangliosidosis and Morquio B disease: expression analysis of missense mutations affecting the catalytic site of acid β-galactosidase. Hum Mut 30:1–8.

Hofer D, Paul K, Fantur K, Beck M, Rouberge A, Vellodi A, Poorthuis BJ, Michelakakis H, Plecko B, Paschke E. 2010. Phenotype determining alleles in G_{M1}-gangliosidosis patients bearing novel *GLB1* mtutations. Clin Genet 78: 236–246.

Ichimura Y, Kumanomidou T, Sou YS, Mizushima T, Ezaki J, Ueno T, Kominami E, Yamane T, Tanaka K, Komatsu M. 2008. Structural basis for sorting mechanism of p62 in selective autophagy. J Biol Chem 283:22847–22857.

Iwasaki H, Watanabe H, Iida M, Ogawa S, Tabe M, Higaki K, Nanba E, Suzuki Y. 2006. Fibroblast screening for chaperone therapy in β-galactosidosis. Brain Dev 28:482–486.

Jeyakumar M, Thomas R, Elliot-Smith E, Smith DA, van der Spoel AC, d'Azzo A, Perry VH, Butters TD, Dwek RA, Platt FM. 2003. Central nervous system inflammation is a hallmark of pathogenesis in mouse models of GM1 and GM2 gangliosidosis. Brain 126:974–987.

Jo H, Yugi K, Ogawa S, Suzuki Y, Sakakibara Y. 2010. Molecular basis of chemical chaperone effects of *N*-octyl-β-valienamine on human β-glucosidase in low/neutral pH conditions. J Proteomics Bioinform 3:104–112.

Kang TS, Stevens RC. 2009. Structural aspects of therapeutic enzymes to treat metabolic disorders. Hum Mut 30:1591–1610.

Komatsu M, Waguri S, Koike M, Sou YS, Ueno T, Hara T, Mizushima N, Iwata J, Ezaki J, Murata S, Hamazaki J, Nishito Y, Iemura S, Natsume T, Yanagawa T, Uwayama J, Warabi E, Yoshida H, Ishii T, Kobayashi A, Yamamoto M, Yue Z, Uchiyama Y, Kominami E, Tanaka K. 2007. Homeostatic levels of p62 control cytoplasmic inclusion body formation in autophagy-deficient mice. Cell 131: 1149–1163.

Lemieux MJ, Mark BL, Cherney MM, Withers SG, Mahuran DJ, James MN. 2006. Crystallographic structure of human beta-hexosaminidase A: interpretation of Tay-Sachs mutations and loss of GM2 ganglioside hydrolysis. J Mol Biol 359: 913–929.

Lieberman RL, D'aquino JA, Ringe D, Petsko GA. 2009. Effects of pH and iminosugar pharmacological chaperones on lysosomal glycosidase structure and stability. Biochemistry 48:4816–4827.

Lin H, Sugimoto Y, Ohsaki Y, Ninomiya H, Oka A, Taniguchi M, Ida H, Eto Y, Ogawa S, Matsuzaki Y, Sawa M, Inoue T, Higaki K, Nanba E, Ohno K, Suzuki Y. 2004. *N*-octyl-beta-valienamine up-regulates activity of F213I mutant beta-glucosidase in cultured cells: a potential chemical chaperone therapy for Gaucher disease. Biochim Biophys Acta 1689:219–228.

Luciani A, Villella VR, Esposite S, Brunetti-Pierri N, Medina D, Settembre C, Gavina M, Pulze L, Giardino I, Pettoello-Mantovani M, D'Apolito M, Guido S, Masliah E, Spencer B, Quaratino S, Raja V, Ballabio A, Maiuri L. 2010. Defective CFTR induces aggresome formation and lung inflammation in cystic fibrosis through ROS-mediated autophagy inhibition. Nat Cell Biol 12:863–875.

Marks DL, Pagano RE. 2002. Endocytosis and sorting of glycosphingolipids in sphingolipid storage disease. Trends Cell Biol 12:605–613.

Matsuda J, Suzuki O, Oshima A, Ogura A, Noguchi Y, Yamamoto Y, Asano T, Takimoto K, Sukegawa K, Suzuki Y, Naiki M. 1997. β-Galactosidase-deficient mouse as an animal model for G_{M1}-gangliosidosis. Glycoconj J 15:729–736.

Matsuda J, Suzuki O, Oshima A, Yamamoto Y, Noguchi A, Takimoto K, Itoh M, Matsuzaki Y, Yasuda Y, Ogawa S, Sakata Y, Nanba E, Higaki K, Ogawa Y, Tominaga L, Ohno K, Iwasaki H, Watanabe H, Brady RO, Suzuki Y. 2003. Chemical chaperone therapy for brain pathology in G_{M1}-gangliosidosis. Proc Natl Acad Sci USA 100:15912–15917.

Morreau H, Galjart NJ, Gillemans N, Willemsen R, van der Horst GT, d'Azzo A. 1989. Alternative splicing of beta-galactosidase mRNA generates the classic lysosomal enzyme and a beta-galactosidase-related protein. J Biol Chem 264: 20655–20663.

Mosna G, Fattore S, Tubiello G, Brocca S, Trubia M, Gianazza E, Gatti R, Danesino C, Minelli A, Piantanida M. 1992. A homozygous missense arginine to histidine substitution at position 482 of the beta-galactosidase in an Italian infantile GM1-gangliosidosis patient. Hum Genet 90:247–250.

Nishimoto J, Nanba E, Inui K, Okada S, Suzuki K. 1991. GM1-gangliosidosis (genetic beta-galactosidase deficiency): identification of four mutations in different clinical phenotypes among Japanese patients. Am J Hum Genet 49: 566–574.

Ogawa S, Matsunaga YK, Suzuki Y. 2002. Chemichal modification of the β-glucocerebrosidase inhibitor *N*-octyl-β-valienamine: synthesis and biological evaluation of 4-epimeric and 4-O-(β-D-galactopyranosyl) derivatives. Bioorg Med Chem 10:1967–1972.

Oshima A, Tuji A, Nagao Y, Sakuraba H, Suzuki Y. 1988. Cloning, sequencing, and expression of cDNA for human beta-galactosidase. Biochem Biophys Res Commun 157:238–244.

Oshima A, Ishii N, Suzuki Y, Osawa M, Sakuraba H. 1995. Beta-galactosidosis (genetic beta-galactosidase deficiency): clinical and genetic heterogeneity of the skeletal form. Dev Brain Dysfunt 8:40.

Oshima A, Yoshida K, Shimmoto M, Fukuhara Y, Sakuraba H, Suzuki Y. 1991. Human beta-galactosidase gene mutations in morquio B disease. Am J Hum Genet 49:1091–1093.

Otomo T, Higaki K, Nanba E, Ozono K, Sakai N. 2009. Inhibition of autophagosome formation restores mitochondrial function in mucolipidosis II and II skin fibroblasts. Mol Genet Metab 98:393–399.

Parenti G. 2010. Treating lysosomal storage diseases with pharmacological cheprones: from concept to clinics. EMBO Mol Med 1:268–279.

Paschke E, Milos I, Kreimer-Erlacher H, Hoefler G, Beck M, Hoeltzenbein M, Kleijer W, Levade T, Michelakakis H, Radeva B. 2001. Mutation analyses in 17 patients with deficiency in acid beta-galactosidase: three novel point mutations and high correlation of mutation W273L with Morquio disease type B. Hum Genet 109:159–166.

Puri V, Watanabe R, Dominguez M, Sun X, Wheatley CL, Marks DL, Pagano RE. 1999. Cholesterol modulates membrane traffic along the endocytic pathway in sphingolipid storage diseases. Nat Cell Biol 1:386–388.

Rempel BP, Clarke LA, Withers SG. 2005. A homology model for human alpha-l-iduronidase: insights into human disease. Mol Genet Metab 85:28–37.

Sanchez P, De Carcer G, Sandoval IV, Moscat J, Diaz-Meco MT. 1998. Localization of atypical protein kinase C isoforms into lysosome-targeted endosomes through interaction with p62. Mol Cell Biol 18:3069–3080.

Sano R, Annunziata I, Patterson A, Moshiach S, Gomero E, Opferman J, Forte M, d'Azzo A. 2009. GM1-ganglioside accumulation at the mitochondria-associated ER membranes links ER stress to Ca(2+)-dependent mitochondrial apoptosis. Mol Cell 36:500–511.

Santamaria R, Blanco M, Chabás A, Grinberg D, Vilageliu L. 2007. Identification of 14 novel GLB1 mutations, including five deletions, in 19 patients with GM1 gangliosidosis from South America. Clin Genet 71:273–279.

Santamaria R, Chabás A, Coll MJ, Miranda CS, Vilageliu L, Grinberg D. 2006. Twenty-one novel mutations in the *GLB1* gene identified in a large group of GM1-gangliosidosis and Morquio B patients: possible common origin for the prevalent p.R59H mutation among gypsies. Hum Mutat 27:1060.

Sawkar AR, Cheng WC, Beutler E, Wong CH, Balch WE, Kelly JW. 2002. Chemical chaperones increase the cellular activity of N370S beta-glucosidase: a therapeutic strategy for Gaucher disease. Proc Natl Acad Sci USA 99:15428–15433.

Settembre C, Fraldi A, Jahreiss L, Spampanato C, Venturi C, Medina D, de Pablo R, Tacchetti C, Rubinsztein DC, Ballabio A. 2008. A block of autophagy in lysoosmal storage disorders. Hum Mol Genet 17:119–129.

Silva CM, Severini MH, Sopelsa A, Coelho JC, Zaha A, d'Azzo A, Giugliani R. 1999. Six novel beta-galactosidase gene mutations in Brazilian patients with GM1-gangliosidosis. Hum Mutat 13:401–409.

Sugii S, Reid P, Ohgami N, Du H, Chang TY. 2003. Distinct endosomal compartments in early trafficking of low density lipoprotein-derived cholesterol. J Biol Chem 278:27180–27189.

Suzuki Y, Ichinomiya S, Kurosawa M, Ohkubo M, Watanabe H, Iwasaki H, Matsuda J, Noguchi Y, Takimoto K, Itoh M, Tabe M, Iida M, Kubo T, Ogawa S, Nanba E, Higaki K, Ohno K, Brady RO. 2007. Chemical chaperone therapy: clinical effect in murine G_{M1}-gangliosidosis. Ann Neurol 62:671–675.

Suzuki Y, Nanba E, Matsuda J, Higaki K, Oshima A. 2008. β-Galactosidase deficiency (β-galactosidosis): GM1-gangliosidosis and Morquio B disease. In: Valle D, Beaudet AL, Vogelstein B, Kinzler KW, Antoanarakis SF, editors. The online metabolic and molecular bases of inherited disease. New York: McGraw-Hill, Chapt. p 151.

Suzuki Y, Ogawa S, Sakakibara Y. 2009. Chaperone therapy for neuronopathic lysosomal diseases: competitive inhibitors as chemical chaperones for enhancement of mutant enzyme activities. Perspect Med Chem 26:7–19.

Takamura A, Higaki K, Kajimaki K, Otsuka S, Ninomiya H, Matsuda J, Ohno K, Suzuki Y, Nanba E. 2008. Enhanced autophagy and mitochondrial aberrations in murine G_{M1}-gangliosidosis. Biochem Biophys Res Commun 367: 616–622.

Takaura N, Yagi T, Maeda N, Nanba E, Oshima A, Suzuki Y, Yamano T, Tanaka A. 2005. Attenuation of ganglioside GM1 accumulation in the brain of G_{M1}-gangliosidosis mice by neonatal intravenous gene transfer. Gene Ther 10: 1487–1493.

Tessitore A, del P Martin M, Sano R, Ma Y, Mann L, Ingrassia A, Laywell ED, Steindler DA, Hendershot LM, d'Azzo A. 2004. GM1-ganglioside-mediated activation of the unfolded protein response causes neuronal death in a neurodegenerative gangliosidosis. Mol Cell 15:753–766.

Adult onset cardiac dilatation in a transgenic mouse line with Galβ1,3GalNAc α2,3-sialyltransferase II (ST3Gal-II) transgenes: a new model for dilated cardiomyopathy

By Osamu SUZUKI,[*1,†] Takao KANAI,[*2] Toshio NISHIKAWA,[*3] Yoshie YAMAMOTO,[*4] Akira NOGUCHI,[*4] Kazuhiro TAKIMOTO,[*5] Minako KOURA,[*1] Yoko NOGUCHI,[*1] Kozue UCHIO-YAMADA,[*1] Shuichi TSUJI[*6] and Junichiro MATSUDA[*1]

(Communicated by Kunihiko SUZUKI, M.J.A.)

Abstract: Sugar chain abnormalities in glycolipids and glycoproteins are associated with various diseases. Here, we report an adult onset cardiac dilatation in a transgenic mouse line with Galβ1,3GalNAc α2,3-sialyltransferase II (ST3Gal-II) transgenes. The transgenic hearts at the end-stage, at around 7 months old, were enlarged, with enlarged cavities and thin, low-tensile walls, typical of dilated cardiomyopathy. Although no apparent change was found in heart gangliosides, glycosylation of heart proteins was altered. Interestingly, sugar moieties not directly related to the ST3Gal-II catalytic reaction were also changed. Significant increases in calreticulin and calnexin were observed in hearts of the transgenic mice. These results suggest that expression of ST3Gal-II transgenes induces abnormal protein glycosylation, which disorganizes the endoplasmic/sarcoplasmic reticulum quality control system and elevates the calreticulin/calnexin level, resulting in suppression of cardiac function. The transgenic mice showed 100% incidence of adult onset cardiac dilatation, suggesting great potential as a new model for dilated cardiomyopathy.

Keywords: ST3Gal-II, cardiac dilatation, calreticulin, calnexin, cardiomyopathy, ER stress

[*1] Laboratory of Animal Models for Human Diseases, National Institute of Biomedical Innovation, Ibaraki, Japan.
[*2] Institute of Laboratory Animals, Tokyo Women's Medical University, Tokyo, Japan.
[*3] Department of Surgical Pathology, Tokyo Women's Medical University, Tokyo, Japan.
[*4] Department of Veterinary Science, National Institute of Infectious Diseases, Tokyo, Japan.
[*5] Division of Experimental Animal Research, National Institute of Infectious Diseases, Tokyo, Japan.
[*6] Institute of Glycoscience, Tokai University, Hiratsuka, Japan.
[†] Correspondence should be addressed: O. Suzuki, Laboratory of Animal Models for Human Diseases, National Institute of Biomedical Innovation, 7-6-8 Saito-Asagi, Ibaraki, Osaka 567-0085, Japan (e-mail: osuzuki@nibio.go.jp).

Abbreviations: ALT: Alanine aminotransferase; AST: Aspartate aminotransferase; ConA: Concanavalin A; CPK: Creatine phosphokinase; DCM: Dilated cardiomyopathy; ER: Endoplasmic reticulum; ERQC: Endoplasmic reticulum quality control; FITC: Fluorescein isothiocyanate; GAPDH: Glyceraldehyde-3-phosphate dehydrogenase; GRP78: 78-kDa Glucose-regulated protein; HCM: Hypertrophic cardiomyopathy; LDH: Lactate dehydrogenase; MAA: *Maackia amurensis* seed lectin; MSGb5: monosialosyl globopentaosylceramide; PNA: Peanut lectin; SGCD: δ-sarcoglycan; SR: Sarcoplasmic reticulum; ST3Gal-I: Galβ1,3GalNAc α2,3-sialyltransferase I (St3gal1); ST3Gal-II: Galβ1,3GalNAc α2,3-sialyltransferase II (St3gal2); TG: homozygous transgenic; WT: wild (non-transgenic).

Introduction

Cardiomyopathy is a serious heart disease, and a heart transplant is the only therapeutic choice in extreme cases. Cardiomyopathies are defined as diseases of the myocardium associated with cardiac dysfunction.[1)] They are classified into five types according to symptomatic features: dilated cardiomyopathy (DCM), hypertrophic cardiomyopathy (HCM), restrictive cardiomyopathy, arrhythmogenic right ventricular cardiomyopathy, and unclassified. Of the five types, DCM and HCM are the most common. In addition, specific cardiomyopathies are also defined as cardiomyopathies with systemic symptoms and/or those secondary to well-defined etiologies, *e.g.*, alcoholism and hypertension. Thus, the etiology of cardiomyopathy is broad and complicated and the development of therapeutic strategies is therefore quite challenging.

Sugar chains in glycolipids and glycoproteins play important roles in many biological processes. Six forms (types I–VI) of β-galactoside α2,3-sialyltransferases have been described so far.[2)–6)] Among them,

doi: 10.2183/pjab.87.550

types I and II are Galβ1,3GalNAc α2,3-sialyltransferases, which mediate the transfer of sialic acid *via* an α2,3-linkage to the galactose residue of terminal Galβ1,3GalNAc structures on *O*-linked oligosaccharides of glycoproteins or glycolipids. The type II enzyme (ST3Gal-II) acts on glycolipids and glycoproteins *in vitro*, but is highly expressed in the brain and has an acceptor substrate preference for glycolipids.[3] This result suggests that the enzyme primarily operates in the biosynthesis of gangliosides, such as GM1b, GD1a, and GT1b.[4),7] The mouse ST3Gal-II gene is developmentally expressed in the heart; it can be detected at 3 days old, but there is only a trace at 21 days and no expression by 49 days.[4] The mouse type I enzyme (ST3Gal-I), which has an acceptor substrate preference for glycoproteins, is slightly expressed in the heart.[8] In humans, ST3Gal-II mRNA is highly expressed in the heart and skeletal muscle, unlike in mice.[9] The physiological significance of strict temporal control and species differences in ST3Gal-II expression remains unknown.

Protein glycosylation is critical for proper protein synthesis. Correct folding of secretory or membrane proteins is achieved in the endoplasmic/sarcoplasmic reticulum (ER/SR) with the aid of various molecular chaperones and oxidoreductases, which are called ER quality control (ERQC) mechanisms.[10] In the system, two lectin-like chaperones, calreticulin and calnexin, bind to monoglycosylated forms of asparagine (N)-linked oligosaccharides. Calreticulin is a soluble Ca^{2+}-binding chaperone, located in the ER lumen.[11] Calnexin is a Ca^{2+}-binding chaperone bound to the ER membrane.[12] Thus, perturbation of protein glycosylation can be estimated by ERQC activity, and the activity can be monitored by measuring the expression levels of calreticulin and calnexin.

During the course of our research on sialic acid metabolism in transgenic mice, we found homozygous-specific, adult onset cardiac dilatation with 100% incidence in mice of a transgenic line harboring ST3Gal-II transgenes. The mice showed altered glycosylation of heart proteins and higher expression of calreticulin in hearts compared with wild-type mice, suggesting that the perturbation in protein glycosylation activated the ERQC machinery, particularly calreticulin expression, and that the high level of calreticulin impairs cardiac function. The mice would serve as a new model for diseases with cardiac dilatation, such as DCM.

Materials and methods

Mice. All mice were housed under specific pathogen-free conditions with food (CMF, Oriental Yeast Co., Ltd., Tokyo, Japan) and water *ad libitum*. C57BL/6CrSlc and Slc:ICR mice were purchased from Japan SLC Inc. (Hamamatsu, Japan). All animal experiments were conducted in accordance with the guidelines for animal experiments of the National Institute of Infectious Diseases, Tokyo, Japan and the National Institute of Biomedical Innovation, Osaka, Japan.

Generation of transgenic mice. The mouse ST3Gal-II cDNA sequence (GenBank: X76989) was cloned in our previous study.[3] The overexpression construct was generated by inserting the cDNA sequence into the multicloning site of a pCAGGS-based plasmid.[13] The *Sal*I-*Bam*HI fragments of the plasmid (Fig. 1A) were injected into the pronuclei of C57BL/6CrSlc zygotes. The manipulated embryos were transferred into the oviducts of pseudopregnant Slc:ICR mice. Tail DNA of transgenic founder mice was first screened by PCR. Integration of the transgene into founder candidates was assessed by Southern blot analysis with *Eco*RI-digested genomic DNA (3 µg/lane) from 4-week-old mice (probe 1: *Sal*I-*Sma*BI fragment of the CAGGS plasmid, 357 bp; probe 2: *Kpn*I-*Xho*I fragment of ST3Gal-II cDNA, 930 bp; Fig. 1A). In our previous study,[14] the insertion site of the transgene was mapped by Blast search for the flanking sequence of the transgene in the Ensembl database (http://www.ensembl.org/, Fig. 1E).

Quantitative analysis of mRNA expressions. The amounts of ST3Gal-II and δ-sarcoglycan (SGCD) mRNA in tissues of 3-month-old mice were examined by quantitative RT-PCR analyses with glyceraldehyde-3-phosphate dehydrogenase (GAPDH) mRNA as an internal control. Total RNA was extracted from each tissue and cDNA was transcribed from the total RNA with reverse transcriptase (Superscript II, Invitrogen Corp., Carlsbad, CA, U.S.A.). Amounts of transcripts were measured by real-time PCR using 7900HT Fast Real-Time PCR System (Applied Biosystems, Foster City, CA, U.S.A.) with QuantiTect Probe PCR Kits (QIAGEN, Hilden, Germany) and TaqMan probes (Applied Biosystems) for three genes.

Protein extraction. The hearts of TG and WT mice were collected and snap-frozen in liquid nitrogen. Heart proteins were extracted by unfractionated and fractionated methods. Unfractionated heart

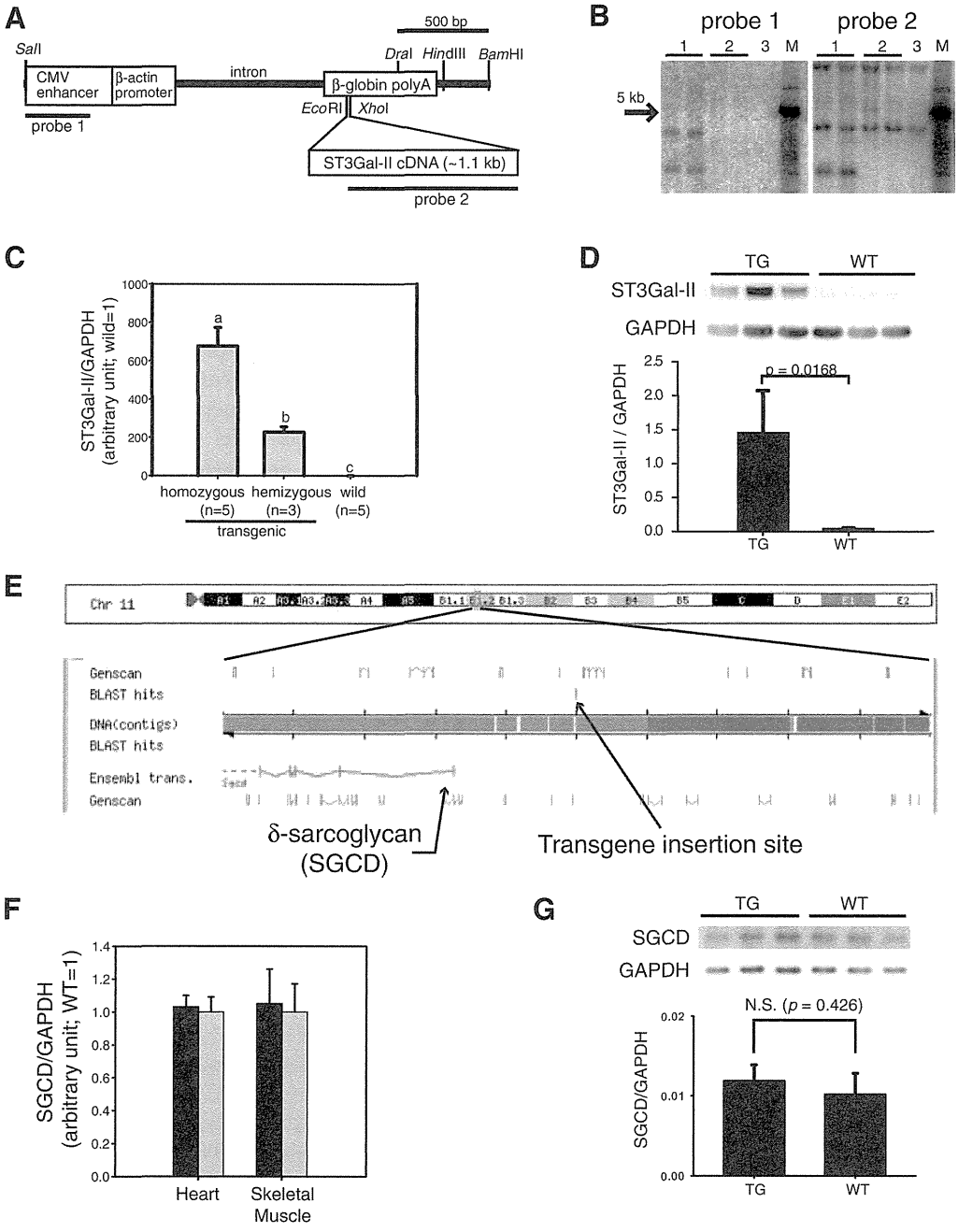

Fig. 1. Production of ST3Gal-II transgenic mice. (A) *SalI-Bam*HI fragments of a pCAGGS-based plasmid containing mouse ST3Gal-II cDNA were injected into mouse zygotes. (B) Integration of the transgene was confirmed by Southern blot analysis. Lane 1: transgenic mice, Lane 2: non-transgenic (WT) mice, Lane 3: C57BL/6Cr. M: DNA size markers. (C) Expression of the transgene was confirmed by TaqMan based quantitative RT-PCR analysis of hearts from homozygous ($n = 5$), hemizygous ($n = 3$), and wild ($n = 5$) mice at 3 months of age. ST3Gal-II expression was normalized with GAPDH expression and displayed as mean ± S.D. with the average of wild values as 1. Values with different labels (a, b, and c) are significantly different ($p < 0.05$). (D) Western blot analysis indicated significantly higher expression (*, $p < 0.05$) of ST3Gal-II protein in homozygous TG hearts than WT hearts at 10 weeks of age ($n = 3$). (E) Our previous study[14] indicated that the transgene was inserted at ~200 kb upstream of the SGCD gene. (F) No significant difference in the SGCD expressions in hearts or skeletal muscles (rectus femoris) between TG ($n = 4$, black bars) and WT ($n = 5$, white bars) was found by TaqMan based quantitative RT-PCR analysis of 3-month-old mice. SGCD expression was normalized with GAPDH expression and displayed as mean ± S.D. with the average of wild values as 1. (G) Western blot analysis indicated no significant difference in expression of δ-sarcoglycan protein between TG and WT hearts at 10 weeks of age ($n = 3$).

proteins were collected with the ReadyPrep Protein Extraction kit (Total protein, Bio-Rad, Hercules, CA, U.S.A.) for quantitative Western blot analysis according to the manufacturer's protocol. Briefly, each heart was homogenized in 1 mL of extraction buffer (7 M urea, 2 M thiourea, 1% ASB-14, 40 mM Tris, 0.001% bromophenol blue) using a bead mill (TissueLyzer, QIAGEN). The homogenate was centrifuged (15,000 × g, 5 min), and the supernatant (TP) was collected for further analysis. Fractionated heart proteins were extracted sequentially for lectin blot analysis with the ReadyPrep kit (Bio-Rad), according to the manufacturer's protocol. Briefly, each heart was homogenized in 1 mL of Buffer 1 (40 mM Tris, pH 7.4) supplemented with Complete Protease Inhibitor Mixture (Roche Diagnostics GmbH, Mannheim, Germany) using a bead mill. The homogenate was centrifuged (15,000 × g, 5 min), the supernatant (fraction 1) was collected, and the pellet was re-suspended in 500 µL of Buffer 2 (8 M urea, 4% CHAPS, 40 mM Tris, 2 mM tributylphosphine). After centrifugation, the supernatant (fraction 2) was collected. The protein concentration of each sample was measured with the EZQ Protein Quantitation kit (Invitrogen).

Quantitative Western blot analysis. The amounts of ST3Gal-II, δ-sarcoglycan, calreticulin, and calnexin in unfractionated heart proteins were examined by quantitative Western blot analyses with GAPDH as an internal control. Heart proteins were separated by 4–12% Bis-Tris gel electrophoresis with MES SDS running buffer (Invitrogen), and transferred onto PVDF membranes (Pall Corp., Port Washington, NY, U.S.A.). Immunoblots were performed using SNAP i.d. (Millipore Corp., Billerica, MA, U.S.A.). The membranes were incubated with primary antibodies against ST3Gal-II (rabbit; Lifespan BioSciences, Inc., Seattle, WA, U.S.A.), δ-sarcoglycan (rabbit; Santa Cruz Biotechnology, Santa Cruz, CA, U.S.A.), calreticulin (goat; Santa Cruz Biotechnology) or calnexin (rabbit; Cell Signaling Technology, Beverly, MA, U.S.A.) and then the blots were visualized by chemiluminescence (ECL-plus, GE Healthcare U.K. Ltd., Buckinghamshire, U.K.) with horseradish peroxidase (HRP)-conjugated secondary antibodies against rabbit (Vector Laboratories Inc., Burlingame, CA, U.S.A.), or goat IgG (Jackson ImmunoResearch laboratories Inc., West Grove, PA, U.S.A.). Blot images were captured by a CCD camera (LAS-3000, Fujifilm, Tokyo, Japan). Then, all blots were treated with WB stripping solution (Nacalai Tesque, Kyoto, Japan), incubated with mouse anti-GAPDH antibodies (Millipore), and visualized by chemiluminescence with HRP-conjugated secondary antibodies against mouse IgG (Jackson ImmunoResearch). Blot images were captured with a CCD camera. The band intensities in each image were measured with imaging software (Multigauge, Fujifilm). The amounts of each protein were calculated as protein/GAPDH ratios.

Clinical observations. The health status of both TG and WT mice was monitored every week for 1 year. The body weights of three male and three female WT and homozygous TG mice were also measured every week from age 40 to 300 days. The TG homozygous mice with dyspnea were used for pathological examinations. WT mice of the same age were used as controls. At necropsy, plasma samples were collected for plasma biochemical analyses using the DRI-CHEM 3000V system (Fujifilm Medical Co. Ltd., Tokyo, Japan).

Pathological examination. Mice were deeply anesthetized with pentobarbital-sodium (Nembutal, Abbott, Chicago, IL, U.S.A.). Then, a thoracotomy was performed. After resecting the thymus, macroscopic photographs were taken to measure cardiac sizes against the thorax width. With these width parameters, we calculated cardiac dilatation indices similar to cardiac thoracic ratios, which are often used at diagnosis with chest radiographs. The thoracic and abdominal cavities were also examined. The vena cava was then resected, and the left ventricle was perfused with PBS and then reperfused with a 7:3 mixture of 10% neutral-buffered formalin and Carnoy fluid. Hearts were removed and fixed in neutral buffered formalin to present four-chamber views. The hearts were embedded in paraffin using conventional methods, cut into 3-µm slices, and specimens were prepared with hematoxylin and eosin staining. Microscopic images were captured under a light microscope (BX50, Olympus Corp., Tokyo, Japan) with a CCD camera (DP25, Olympus).

Ganglioside analysis. Ganglioside fractions were obtained from heart, cerebrum and liver by the Folch extraction and partition of total lipids.[15] The pooled upper phase was saponified with 0.5 mL of 0.2 N KOH/methanol and desalted with a Sep-Pak C18 reverse-phase cartridges (Waters Corp., Milford, MA, U.S.A.).[16] Individual gangliosides were separated by thin-layer chromatography on a plate coated with super-fine silica gel 60 (Merck KGaA, Darmstadt, Germany) with chloroform:methanol:0.2% $CaCl_2$ (60:35:8, by volume) and visualized with resorcinol reagent.[17]

Lectin blot analysis of heart proteins. Two protein fractions from 10-week-old TG and WT mice (~2 μg/lane) were separated by 4–12% Bis-Tris gel electrophoresis with MES SDS running buffer (Invitrogen), transferred onto PVDF membranes (Pall). The protein transfer onto PVDF membranes was confirmed using a SYPRO Ruby blot stain kit (Invitrogen) before the lectin blots and the images were captured by a laser scanner (FX-Pro, Bio-Rad). Lectin binding assays were performed using SNAP i.d. (Millipore). For MAA assays, digoxygenin (DIG)-conjugated lectins (MAA) included in the DIG glycan differentiation kit (Roche Diagnostics) were used with HRP-conjugated anti-DIG antibody (Jackson ImmunoResearch). For ConA and PNA blots, fluorescein-conjugated ConA and PNA (Vector Laboratories) were used with HRP-conjugated anti-fluorescein antibody (Vector Laboratories). All blots were visualized with chemiluminescence (ECL-plus) and their images were captured with a CCD camera.

Lectin staining of heart and skeletal muscle tissues. The sugar-chain status in frozen sections (6 μm) of hearts and rectus femoris muscles at 10 weeks of age was analyzed by binding of biotinylated PNA lectins (Vector Laboratories); the sections were treated with or without α2,3-sialidase (5 U/mL, Takara Bio Inc., Otsu, Japan). The lectins were visualized by 0.1 mg/mL FITC-avidin D (Vector Laboratories) under a fluorescence microscope (OPTIPHOTO, Nikon Corp., Tokyo, Japan) with a digital image capture unit (DXC-S500/OL, Olympus).

Statistical analyses. Expressions of ST3Gal-II mRNA (Fig. 1C) were analyzed statistically among three genotypes using analysis of variance, followed by pairwise comparisons by the Tukey–Kramer method. Expressions of SGCD mRNA (Fig. 1F) and proteins (Figs. 1D, 1G, 6C, and 6D), the heart and body weight parameters (Fig. 2E), and biochemical analyses (Fig. 2F) were analyzed statistically between TG and WT mice using Student's *t*-test. Differences with a $p < 0.05$ were considered statistically significant. All statistical analyses were conducted using StatView Version 5 (SAS Institute Inc., Cary, NC, U.S.A.).

Results

Generation of transgenic mice. Of two established transgenic lines (4C30 and 4C59), mice only from 4C30 line exhibited cardiac dilatation and was used for further studies. The presence of the transgenes (Fig. 1A) was confirmed by Southern blot analysis (Fig. 1B), and their expression was confirmed by quantitative RT-PCR (Fig. 1C) and Western blot analyses (Fig. 1D). Extremely higher levels of ST3Gal-II expression were found in hearts of transgenic mice than in those of wild mice. The mRNA level of ST3Gal-II in the heart was approximately three times higher in homozygous transgenic mice than in hemizygous transgenic mice. Our previous study[14] showed that the transgene was inserted at upstream of the δ-sarcoglycan (SGCD) gene (Fig. 1E). However, neither mRNA nor protein expression of SGCD gene in hearts was influenced by genotype (Figs. 1F and 1G).

Clinical observations. All mice of the homozygous transgenic (TG) line developed severe cardiac dilatation with dyspnea, deformation of the thorax, and rapid weight loss at the end-stage (Fig. 2A). Both wild-type (non-transgenic; WT) and hemizygous transgenic animals survived without abnormal symptoms for at least 1 year. The TG mice were born healthy and grew normally until approximately 150 days (Fig. 2B, 2C). At that point, they exhibited rapid weight loss and died about a week after the onset of symptoms. The average life span of the TG mice was 227 ± 55 days (mean ± SD, Fig. 2D). Approximately one-third of hemizygous transgenic mice older than 18-months also showed similar, but milder, cardiac symptoms compared with the homozygous transgenic mice (data not shown). Significantly increased heart:body weight ratios, indicating heart enlargement, were already evident in the TG mice at 4 weeks of age in comparison with WT mice even though the TG mice showed no clinical symptoms (Fig. 2E). Biochemical analyses indicated that the plasma CPK and LDH values were significantly higher in TG mice than in WT mice at 4 weeks of age, long before the onset of symptoms (Fig. 2F).

Pathological examination. At necropsy of the TG mice, the hearts were enlarged and occupied a larger area inside the thorax, with all four chambers dilated and thin, with low tensile-strength walls (Fig. 3). Both atria and ventricles of TG hearts were larger compared with those of the WT hearts. From the width measurement of hearts and thoraxes, we calculated cardiac dilatation indices. Mice at 5–6 months of age in the TG group showed significantly larger indices (0.66 ± 0.44; mean ± SD, $n = 4$, range, 0.628–0.723) than those in the WT group (0.451 ± 0.039, $n = 3$, range, 0.408–0.485). Observation of the four chambered view of the heart presented extremely thin atrial walls in the TG group, with a high

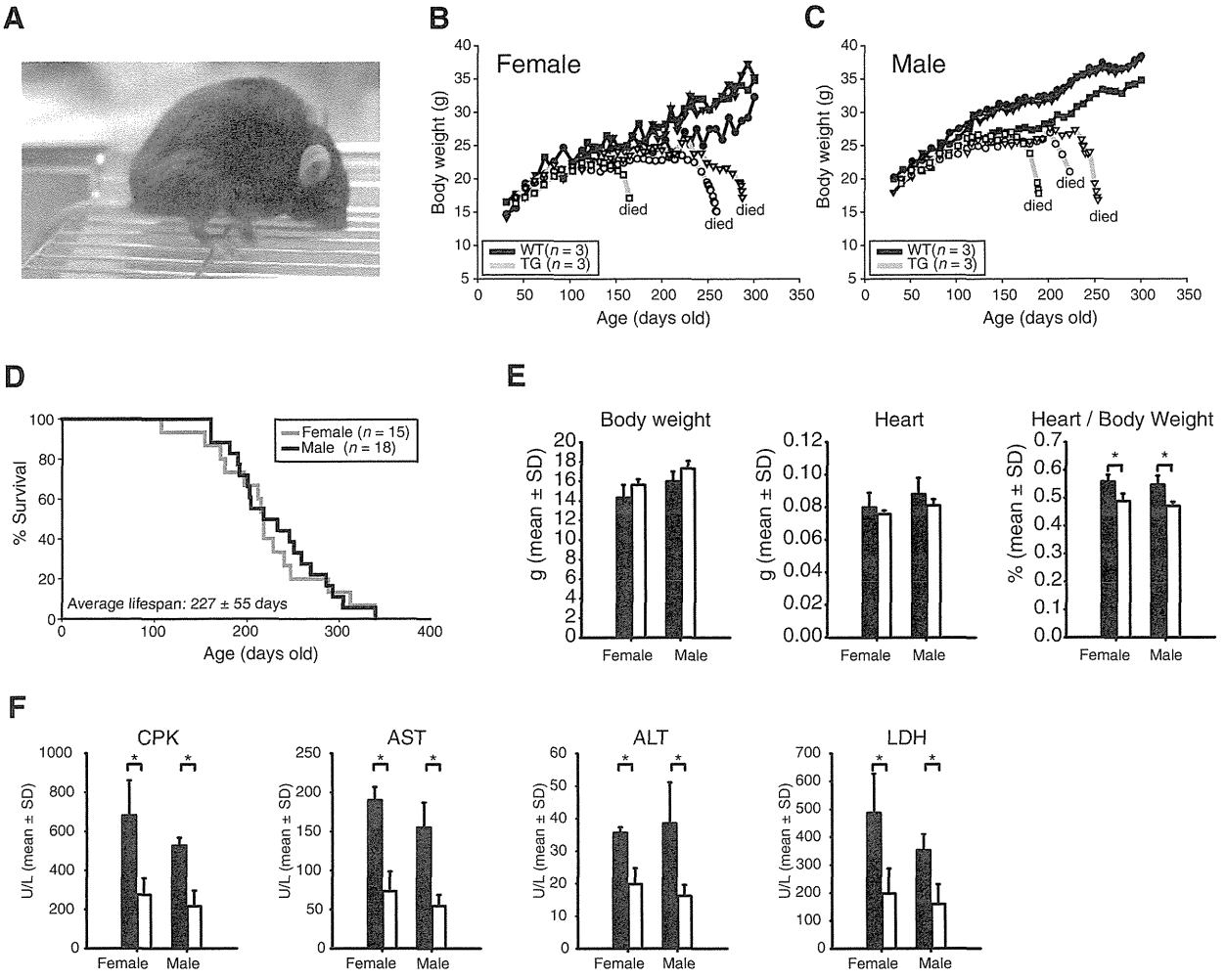

Fig. 2. (A) Appearance of 6-month-old transgenic (TG) mice homozygous for the ST3Gal-II transgene. Daily body weights gains (B, C) in TG and WT mice. (D) Kaplan–Meier survival plot for male and female TG mice. All hemizygous transgenic and WT mice survived until at least 1 year old (not plotted). (E) Body weights, heart weights, and heart:body weight ratios of TG (black bars) and WT (white bars) mice at 4 weeks of age (mean + SD; $n = 3$). (F) Biochemical analysis of mouse plasma enzymes (mean + SD; $n = 5$). Four enzyme activities were compared in plasma samples from TG (black bars) and WT (white bars) mice at 4 weeks of age. All plasma enzymes tested showed significantly higher activities in TG mice than in WT mice, even at a young age, long before the onset of symptoms. Asterisks in E and F indicate significant difference between WT and TG mice ($n = 3$; $p < 0.05$).

degree of dilatation and blood filling into the inner space. The left and right ventricles also exhibited thin free walls and septal walls with a high degree of dilatation. The papillary muscles in the left ventricles had also become thin. Except for pulmonary and hepatic congestion, no abnormality was found in the thoracic or abdominal cavities.

Our histological observations revealed that the width of myocardial fibers changed in both left and right atria as well as ventricular myocardial layers in TG hearts (Fig. 4). Particularly in ventricular muscles, thin and thick fibers were mixed, presenting a degenerated and irregular orientation. In the myocardium layer, connective tissues with slight fibrosis were sporadically observed, but there was no cell infiltration. No coronary artery in the atrium, ventricle, or myocardium presented with luminal narrowing or obstruction. No apparent abnormality was found in the myocardium of WT hearts. A survey of 45 additional organs in TG mice by hematoxylin and eosin staining revealed severe blood congestion in the lungs, liver, and spleen, and a slight, mild degeneration in skeletal muscles but no remarkable alteration in other organs (data not shown).

Ganglioside analysis. High-performance thin-layer chromatography analysis showed no difference

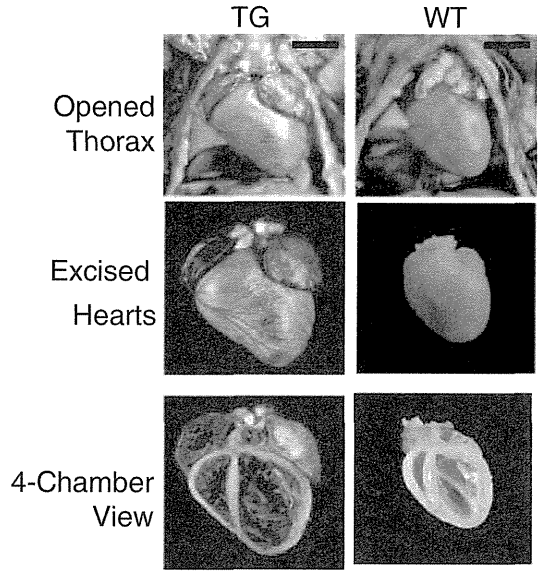

Fig. 3. The hearts of 6-month-old transgenic (TG) mice homozygous for the ST3Gal-II transgene were much larger than those of wild-type (WT) mice. TG heart shows severe dilatation of all four chambers with thin, low tensile-strength walls. Bars = 5 mm.

in the ganglioside composition in the heart, brain, or liver between the TG and WT mice (Fig. 5).

Lectin blot analysis of heart proteins. Alterations in the sugar moieties of heart glycoproteins were examined by lectin blot staining in two fractions of heart proteins from 10-week-old mice (Fig. 6A, 6B). Three lectins were used: *Maackia amurensis* seed lectins (MAA) recognize α2,3-sialylation of sugars, such as Gal-GalNAc; peanut lectins (PNA) recognize non-sialylated Gal-GalNAc sugars; concanavalin A (ConA) recognizes high-mannose-type sugars. Staining with MAA and PNA lectins indicated that heart proteins of TG mice were less sialylated than those of WT mice, even though ST3Gal-II was overexpressed in the TG mice. One differentially stained ConA band was found in fraction 1 (soluble proteins containing cytosolic proteins), indicating that some cytosolic heart proteins in TG mice lost their high-mannose-type glycosylation, which was present in those of WT mice.

Calreticulin and calnexin expression in hearts. Quantitative Western blots with TG and

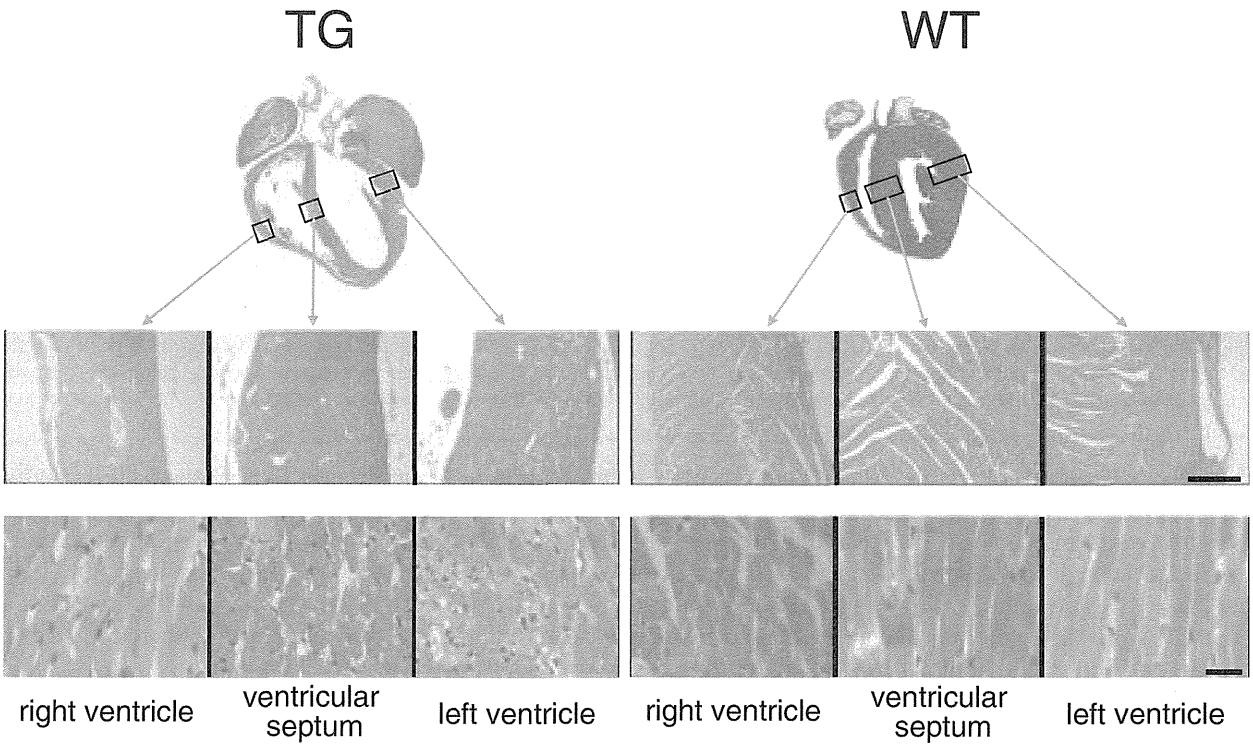

Fig. 4. Histopathological observations of hearts in 6-month-old transgenic (TG) and wild-type (WT) mice. Hematoxylin and eosin-stained tissue sections from three cavity walls, the positions of which are indicated by rectangles in the upper images and are shown in low (middle images, bar = 100 µm) and high (lower images, bar = 10 µm) magnifications. Slight fibrosis was observed sporadically in TG hearts, but no apparent cell infiltration was found in either TG or WT hearts.

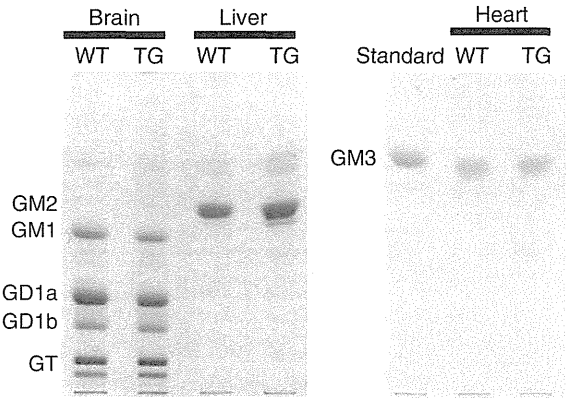

Fig. 5. Ganglioside analysis in the brain, liver, and heart. No difference in ganglioside composition was found in the brain, liver, or heart between 6-month-old transgenic (TG) and wild-type (WT) mice, as analyzed by thin-layer chromatography and resorcinol staining. The amounts of gangliosides per lane were equivalent to 1.5 mg, 5 mg, and 5 mg dry weight of the brain, liver and heart, respectively.

WT heart proteins at 10 weeks of age revealed a significant increase ($p < 0.05$) in the amounts of calreticulin and calnexin in the TG heart (Fig. 6C, 6D).

Lectin staining of heart and skeletal muscle tissues. Sialylation in heart and skeletal muscle tissues with transgene-derived ST3Gal-II was examined by histochemical analysis using PNA lectin in combination with α2,3-sialidase treatment (Fig. 7). The ST3Gal-II enzyme converts sugars (Galβ1,3GalNAc) that are bound by PNA to sugars (SialGalβ1, 3GalNAc) that are not bound by PNA by α2,3-sialylation of terminal galactose residues. The α2,3-sialidase enzyme reverses the reaction. In the heart, the staining was essentially the same between TG and WT mice with and without α2,3-sialidase treatment. In contrast, PNA staining in the TG skeletal muscle tissue was more intense than that in the WT tissue even without α2,3-sialidase treatment. Staining in skeletal muscle tissue was essentially the same between TG and WT mice after the α2,3-sialidase treatment. These results indicated that most of the terminal Galβ1,3GalNAc structures in pericellular regions (cell membranes and ECM) were sialylated *via* the α2,3 linkage of galactose residues in the heart. The sialylation decreased in skeletal muscle of TG mice compared with that in WT mice. After α2,3-sialidase treatment, the TG and WT tissues showed similar staining patterns, indicating that the differential staining by PNA without α2,3-sialidase treatment was attributable to differential α2,3-sialylation of Gal-GalNAc structures and not different amounts of Gal-GalNAc structures.

Discussion

The mice that were homozygous for the ST3Gal-II transgene developed non-inflammatory cardiac dilatation with relatively late onset and 100% lethality. Our findings suggest a new concept that abnormal glycosylation of heart proteins can cause cardiac dilatation *via* perturbation of ER/SR environments. Thus, the mice may be a new model for examining the mechanism and developing therapeutics of non-inflammatory cardiac dilatation related to abnormal glycosylation.

The severity and onset of cardiac symptoms in 4C30 mice depended on a level of transgene expression. As a 1-year observation revealed that cardiac dilatation in 4C30 mice was homozygous-specific, we first considered two issues with regard to the possible mechanism of the cardiac dilatation: the effect of genome disruption by transgene insertion and the effect of transgene dosage. However, after longer observation and chromosomal mapping of the transgene, we concluded that the effect of the transgene itself was the primary cause for two reasons. First, some hemizygous transgenic mice older than 18 months, about three times older than the homozygous transgenic mice, also showed mild cardiac symptoms, suggesting that a level of transgene expression, about one third in the hemizygous compared to that in the homozygous (Fig. 1C), may be involved in the severity and onset of symptoms. Second, our previous report on chromosomal mapping of the transgene in 4C30 mice by genomic walking[14] indicated that the transgenes were inserted into the B1.2 region of chromosome 11, approximately 200 kb upstream of the δ-sarcoglycan gene (Fig. 1E), an area in which no gene has been reported to date. Decreased δ-sarcoglycan expression was expected in homozygous mice because δ-sarcoglycan is a key component of the sarcomere complex in muscle tissues and its deficiency can cause degenerative heart diseases, including dilated cardiomyopathy.[18] However, δ-sarcoglycan was equally expressed in TG and WT mice (Figs. 1F and 1G), suggesting that the transgene insertion had no adverse effect on genes near the insertion site in TG mice.

The histological analysis indicated that TG mice have cardiac dilatation with a non-inflammatory mechanism. The causes of cardiac dilatation in humans, such as dilated cardiomyopathies, are not

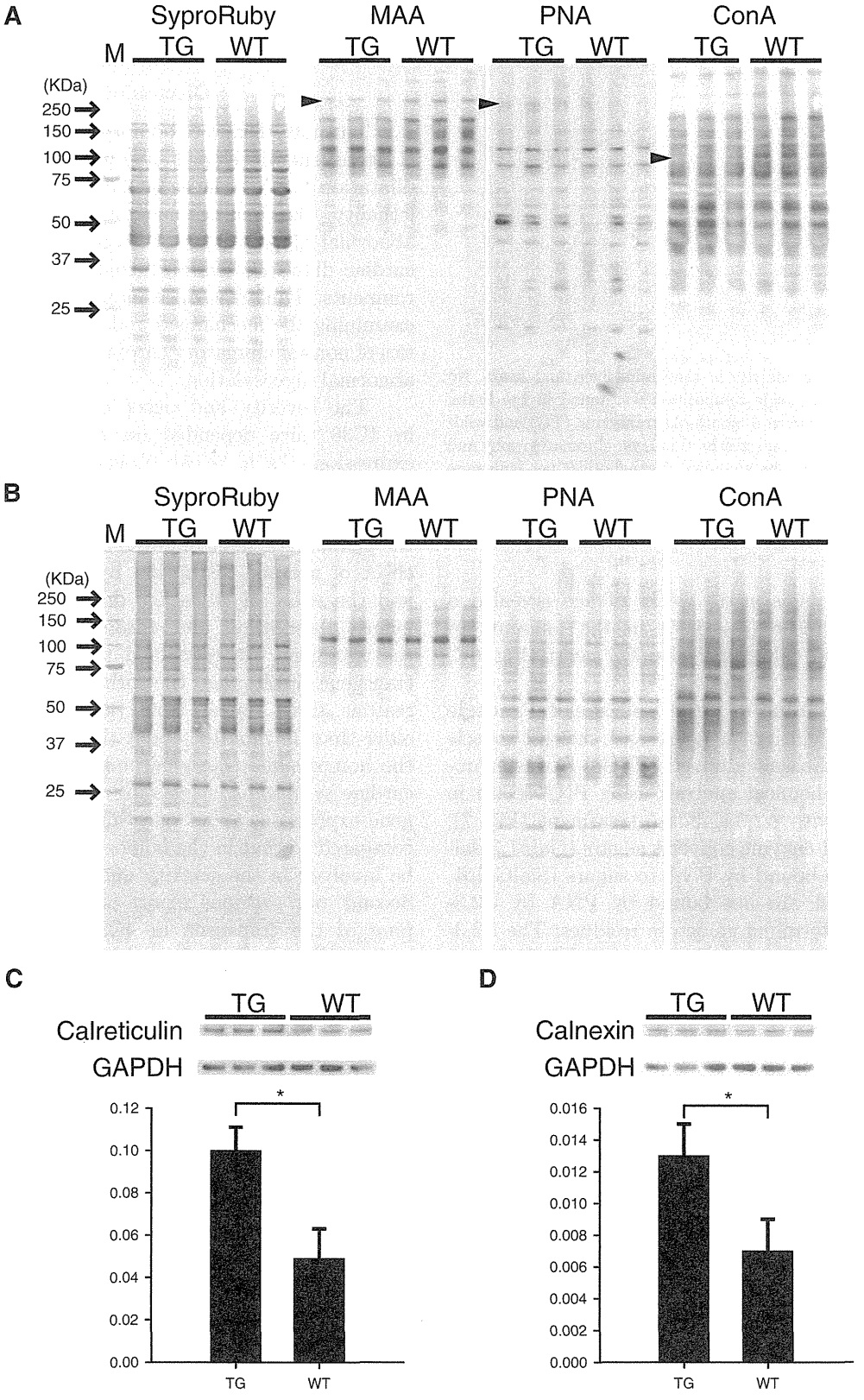

Fig. 6. *Continued on next page.*